Paleoceanography and Paleoclimatology

RESEARCH ARTICLE
10.1029/2018PA003501

Southwest Pacific Vertical Structure Influences on Oceanic Carbon Storage Since the Last Glacial Maximum

Vincent J. Clementi[1] and **Elisabeth L. Sikes**[1]

[1]Department of Marine and Coastal Sciences, Rutgers University, New Brunswick, NJ, USA

Key Points:
- Subantarctic Mode Water was well ventilated during the LGM and throughout the deglaciation
- Glacial CO_2 storage was focused in two layers: an isolated glacial Antarctic Intermediate Water and greater sequestration at deeper depths
- After the LGM, CO_2 was rapidly released from intermediate depths and gradually released from the deep ocean across the deglaciation

Supporting Information:
- Supporting Information S1

Correspondence to:
V. J. Clementi,
clementi@marine.rutgers.edu

Citation:
Clementi, V. J., & Sikes, E. L. (2019). Southwest Pacific vertical structure influences on oceanic carbon storage since the Last Glacial Maximum. *Paleoceanography and Paleoclimatology*, *34*, 734–754. https://doi.org/10.1029/2018PA003501

Received 23 OCT 2018
Accepted 1 APR 2019
Accepted article online 4 APR 2019
Published online 7 MAY 2019

Abstract Lower atmospheric CO_2 concentrations during the Last Glacial Maximum (LGM; 23.0–18.0 ka) have been attributed to the sequestration of respired carbon in the ocean interior, yet the mechanism responsible for the release of this CO_2 during the deglaciation remains uncertain. Here we present calculations of vertical differences in oxygen and carbon isotopes ($\Delta\delta^{18}O$ and $\Delta\delta^{13}C$, respectively) from a depth transect of southwest Pacific Ocean sediment cores to reconstruct changes in water mass structure and CO_2 storage. During the Last Glacial Maximum, $\Delta\delta^{18}O$ indicates a more homogenous deep Pacific below 1,100 m, whereas regional $\Delta\delta^{13}C$ elucidates greater sequestration of CO_2 in two distinct layers: enhanced CO_2 storage at intermediate depths between ~940 and 1,400 m, and significantly more CO_2 at 1,600 m and below. This highlights an isolated glacial intermediate water mass and places the main geochemical divide at least 500 m shallower than the Holocene. During the initial stages of the deglaciation in Heinrich Stadial 1 (17.5–14.5 ka), restructuring of the upper ~2,000 m of the southwest Pacific water column coincided with sea-ice retreat and rapid CO_2 release from intermediate depths, while CO_2 release from the deep ocean was earlier and more gradual than waters above it. These changes suggest that sea-ice retreat and shifts in Southern Ocean frontal locations contributed to rapid CO_2 ventilation from the Southern Ocean's intermediate depths and gradual ventilation from the deep ocean during the early deglaciation.

1. Introduction

Earth's climate underwent substantial changes during the last glaciation, which was in part characterized by atmospheric carbon dioxide (CO_2) concentrations roughly 80 ppm lower than Holocene values (Marcott et al., 2014; Monnin et al., 2001; Parrenin et al., 2013). While no single mechanism can explain the full reduction in CO_2 during the Last Glacial Maximum (LGM), it is generally accepted that most of this CO_2 was sequestered in the ocean interior. Factors contributing to CO_2 drawdown during the LGM include changes in high-latitude overturning circulation, increased carbonate dissolution, a more efficient biological pump, and greater sea-ice extent; similarly, these mechanisms have been invoked as key drivers of CO_2 release from the ocean during the deglaciation (Boyle, 1988; Broecker, 1982; Sigman & Boyle, 2000; Sigman et al., 2010; Stephens & Keeling, 2000).

The Southern Ocean influences atmospheric CO_2 variability and the global carbon system on glacial-interglacial timescales owing to its important role in global overturning circulation, whereby CO_2-rich interior waters upwell to the surface and exchange CO_2 with the atmosphere (e.g., Lynch-Stieglitz et al., 1995; Sigman et al., 2010). Enhanced CO_2 storage at depth during the LGM has been linked to changes in Southern Ocean circulation and structure, a colder, more saline and stratified deep ocean (Adkins et al., 2002), and expanded Antarctic sea-ice extent (Benz et al., 2016; Ferry et al., 2015; Shemesh et al., 2002), all of which could have inhibited upwelled waters from equilibrating with the atmosphere (Adkins et al., 2002; Jansen, 2017; Kobayashi et al., 2015; Lund et al., 2011; Sikes, Cook, et al., 2016; Stephens & Keeling, 2000; Watson et al., 2015). Similarly, changes in the vertical structure of the Southern Ocean are one possible mechanism contributing to the release of CO_2 to the atmosphere during the deglaciation (e.g., Basak et al., 2018; Du et al., 2018; Roberts et al., 2016; Sikes et al., 2017; Skinner et al., 2013), though other mechanisms, such as changes in the efficiency of the biological pump (e.g., Bauska et al., 2016; Hertzberg et al., 2016; Martin, 1990), have also been invoked.

1.1. Oceanographic Setting

In the modern ocean, North Atlantic Deep Water (NADW) is exported south and ultimately enters the Southern Ocean below deep waters sourced from the Indian and Pacific basins (Talley, 2013; Figures 1b and 2). Together, these waters form upper- and lower-Circumpolar Deep Water (CDW), which is zonally transported by the Antarctic Circumpolar Current (Figure 1a). Interactions between positive and negative buoyancy fluxes—owing to freshening/warming or brine rejection/cooling, respectively—and strong westerly winds establish an upper and lower branch of overturning circulation and create a region of divergence where CO_2-rich CDW advects to the surface along steep isopycnal surfaces (Abernathey et al., 2011; Gordon, 1971; Marshall & Speer, 2012; Talley, 2013). Today, the two branches of overturning are separated by an isopycnal boundary that sits at ~2,000 m (Marshall & Speer, 2012; Talley, 2013; Tamsitt et al., 2017). Sea-ice extent partially determines the buoyancy fluxes near Antarctica and is linked to the region of divergence, making it an important factor in the closure of global overturning circulation via the wintertime conversion of upwelled CDW to Subantarctic Mode Water (SAMW), Antarctic Intermediate Water (AAIW), and Antarctic Bottom Water (AABW) (Abernathey et al., 2016; Groeskamp et al., 2016; Saenko et al., 2002; Santoso & England, 2004).

In the Pacific sector, the less dense Upper CDW (UCDW), which is primarily sourced from Pacific Deep Water (PDW), outcrops north of the Polar Front (PF) (Talley, 2013, Figure 1b). This water gains buoyancy from freshening and/or warming and loses CO_2 to the atmosphere before sinking as a significant component of AAIW (~800–1,500 m) near the Subantarctic Front and Subantarctic Mode Water (~400–800 m) near the Subtropical Front (STF) (Belkin & Gordon, 1996; Hartin et al., 2011; Marshall & Speer, 2012; Orsi et al., 1995; Sallee et al., 2006). These two water masses form the upper cell of overturning circulation (e.g., Hanawa & Talley, 2001; Hasson et al., 2012; Piola & Georgi, 1982; Sallee et al., 2010, 2006; Sloyan et al., 2010; Sloyan & Rintoul, 2001; Talley, 2003, Figures 1b and 2). The zonal circulation of the Southern Hemisphere westerlies (SHW) favors a northward transport of Antarctic sea ice, which upon melting creates strong temperature and salinity gradients in the upper water column (fresh and cold meltwater above salty and warm seawater) that facilitate vertical mixing and the formation of AAIW with its characteristic salinity minimum (e.g., Abernathey et al., 2016; Duffy et al., 2001; Groeskamp et al., 2016; Komuro & Hasumi, 2003; Saenko & Weaver, 2001; Santoso & England, 2004). Modern observations of AAIW freshening is attributed to enhanced northward transport and melting of Antarctic sea ice under increasingly warm conditions (Haumann et al., 2016).

South of the PF, the denser NADW-component lower CDW (LCDW) upwells to the surface and only partially equilibrates CO_2 with the atmosphere; cooling and brine rejection from the region of sea-ice extent impart a negative buoyancy flux to form AABW (Gordon, 1971, 2001; Figures 1b and 2). A number of studies have also invoked turbulent mixing as an important process in the closure of the lower cell (e.g., De Lavergne et al., 2017; Garabato et al., 2004; Ito & Marshall, 2008; Ruan et al., 2017), whereby passage of the Antarctic Circumpolar Current over rough topography in the Pacific sector drives turbulent mixing of LCDW toward the lower boundary of overturning in a region of negative buoyancy (De Lavergne et al., 2017; Ruan et al., 2017; Tamsitt et al., 2017; Watson & Naveira Garabato, 2006). In both models, negative buoyancy fluxes are vital for the conversion of LCDW to AABW.

These Southern Ocean water formation regimes feed our study region in the southwest Pacific Ocean, with the formation of SAMW and AAIW in the upper cell influenced by regional oceanographic complexities. It is well established that SAMW and AAIW (often collectively called *intermediate water*) vary somewhat in composition across the Southern Ocean depending on the sector of formation. These waters advect and mix well beyond their formation areas, with recent evidence from ARGO floats and models demonstrating more conclusively that intermediate water formation is not homogenous across the Southern Ocean (Hanawa & Talley, 2001; Hasson et al., 2012; McCartney, 1977; Sallee et al., 2010; Sloyan & Rintoul, 2001; Talley, 2013). Intermediate waters that bathe the New Zealand region are derived from three areas, with about half formed locally in the region south of the Tasman Sea or on the Campbell Plateau, and to a lesser extent waters advected in from the Indian Ocean or formations regions farther west in the Pacific (about one fourth each). These intermediate waters have renewal times on average of less than a decade and combine to form an overwhelmingly northward transport of intermediate water from these formation zones to areas north of our study area (Hasson et al., 2012). Due to the topographical complexities of the area, there is a small

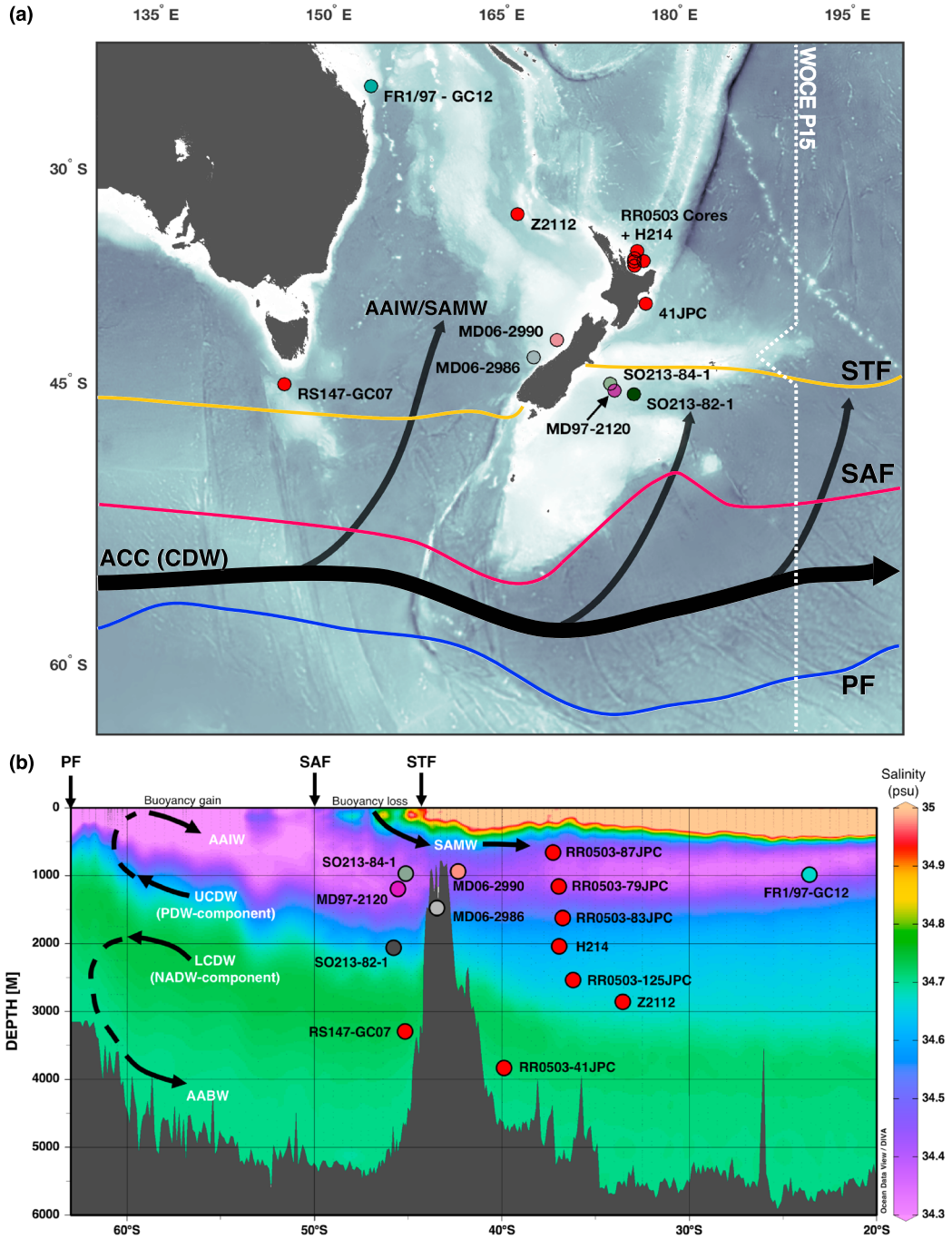

Figure 1. Study area and oceanographic setting. (a) Map showing core locations in this study (red dots; Table S1) and those from published work: MD06-2990 (943 m, pink), SO213-84-1 (972 m, light green), MD06-2986 (1,477 m, gray), SO213-82-1 (2,066 m, dark green) (Ronge et al., 2015); FR1/97-GC12 (990 m, blue; Bostock et al., 2004); and MD97-2120 (1,200 m, purple; Pahnke & Zahn, 2005). Southern Ocean fronts are designated by lines: Subtropical Front (STF; yellow line), Subantarctic Front (SAF; red line), and Polar Front (PF; blue line). The Antarctic Circumpolar Current (ACC; black line) moves water eastward in the Southern Ocean to the south of New Zealand. (b) A latitudinal depth transect of the study area showing regional salinity along the World Ocean Circulation Experiment (WOCE) P15 track at 190°E. Core locations from this study and published work (as in Figure 1a), as well as modern major water masses in the region, are presented on this salinity profile: Subantarctic Mode Water (SAMW); Antarctic Intermediate Water (AAIW); Pacific Deep Water (PDW); North Atlantic Deep Water (NADW); Antarctic Bottom Water (AABW); Upper Circumpolar Deep Water (UCDW); Lower Circumpolar Deep Water (LCDW). Circumpolar Deep Water (CDW) upwells in the Southern Ocean owing to winds and buoyancy forcing. PDW-component UCDW outcrops north of the PF and forms AAIW near the SAF and SAMW near the STF. NADW-component LCDW outcrops south of the PF and sinks as AABW. Generalized overturning routes are indicated by dashed lines.

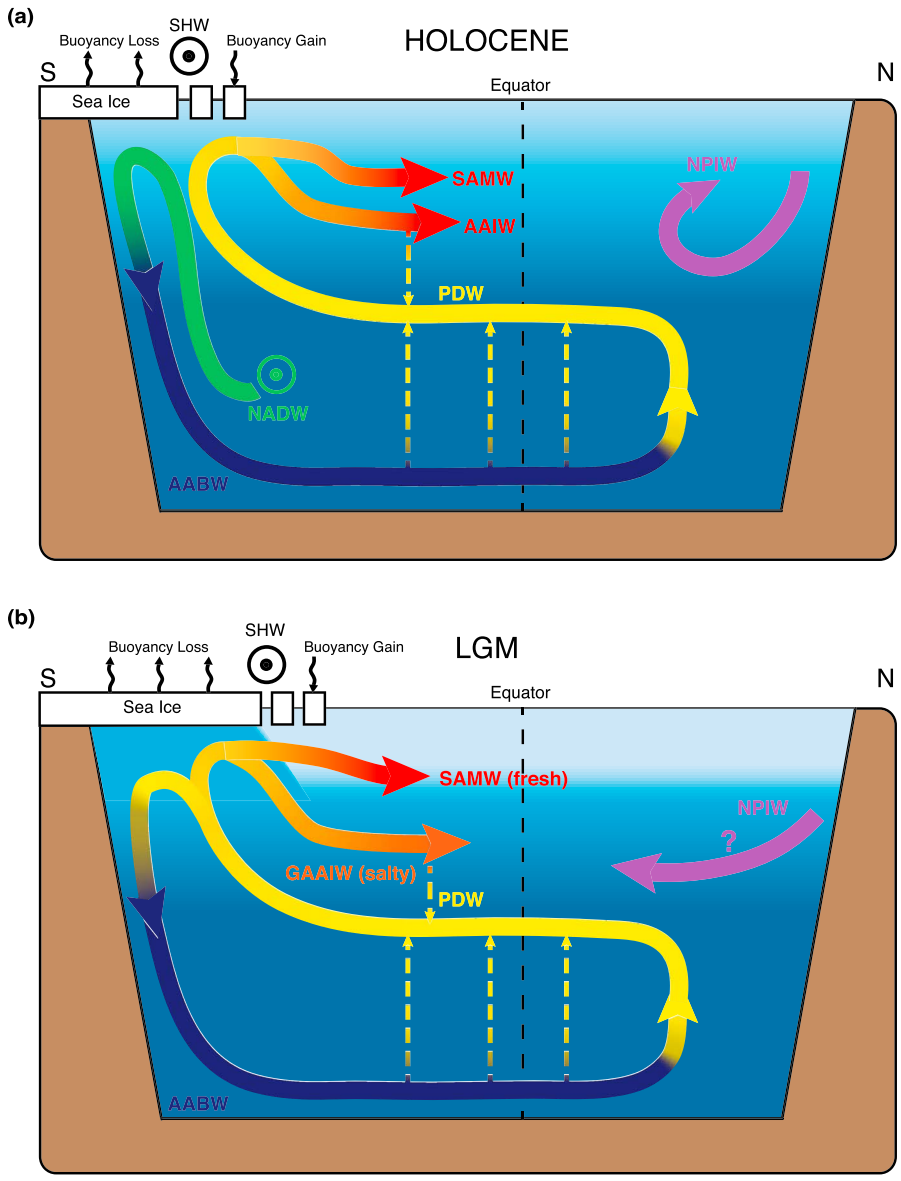

Figure 2. Pacific Ocean circulation regimes during the Holocene and LGM. (a) Modern overturning circulation and water column structure based on Talley (2013). Major water masses are shown: Subantarctic Mode Water and Antarctic Intermediate Water (SAMW/AAIW; red-orange); Pacific Deep Water (PDW; yellow); North Atlantic Deep Water (NADW; green); Antarctic Bottom Water (AABW; blue); North Pacific Intermediate Water (NPIW; purple). Dashed arrows indicate subsurface exchange between water masses. Approximate positions of buoyancy fluxes (black arrows) and the Southern Hemisphere westerlies (SHW, bulls eye) are shown. Today, NADW enters the Southern Ocean and is the main source of water forming AABW, whereas PDW supplies SAMW/AAIW. Sea-ice extent, linked to the Polar Front, establishes a region of negative buoyancy and bottom water formation near Antarctica. The SHW are in a poleward position, which drives upwelling of subsurface waters. (b) Proposed changes in overturning circulation and structure during the LGM. Key differences between the Holocene and LGM include the absence of NADW in the Pacific (Sikes et al., 2017) and greater sea-ice extent. Without NADW input, PDW would have supplied both the upper and lower branches of overturning in the southwest Pacific. Expanded sea ice broadened the region of negative buoyancy and shifted the region of positive buoyancy north, shoaling the locus of stratification to at least 1,100 m and prompting the formation of a saltier Glacial Antarctic Intermediate Water (GAAIW). SAMW during the LGM was formed similar to AAIW today and was likely fresher as it was formed near a region of sea-ice melt (Keeling & Stephens, 2001). An equatorial displacement of the SHW reduced Southern Ocean upwelling (Anderson et al., 2009) but kept SAMW well ventilated (Figure S3). Glacial circulation and structural changes coincided with, and were likely integral, to enhanced CO_2 sequestration at these depths during the LGM. Breakdown of this glacial structure contributed to the release of this CO_2 across the deglaciation.

amount of focused southward recirculation transport of the deeper sitting AAIW along Tasmania in the Tasman Sea and east of New Zealand (e.g., Hasson et al., 2012; Speich et al., 2002). The transport of SAMW and AAIW north of New Zealand can be identified at similar depths to where they are found farther south by using their identifying characteristics such as density, temperature, and salinity, which verify their transport from and continuity with formation zones in the Southern Ocean (Hasson et al., 2012; Rintoul & England, 2002; Sloyan & Rintoul, 2001, Figure S1 in the supporting information). These identifying characteristics of intermediate waters are distinctive enough that they are commonly used where these waters underlie subtropical surface waters to reveal information on the formation areas' atmosphere-ocean winter interactions and circulation (Rintoul & England, 2002).

While direct observations of Southern Ocean structure, circulation, and carbon storage can be made today, geochemical proxies—including the carbon and oxygen isotope composition of seawater, which are recorded in the calcium carbonate shells of foraminifera—are commonly employed to reconstruct past ocean conditions (Charles & Fairbanks, 1992; Curry & Oppo, 2005; Mackensen et al., 1993; Ninnemann & Charles, 2002). The carbon isotopic composition of calcite ($\delta^{13}C$) reflects the dissolved inorganic carbon (DIC) of seawater and, to a lesser extent, temperature (Broecker & Maier-Reimer, 1992; Charles et al., 1993; Curry et al., 1988; Curry & Oppo, 2005; Duplessy et al., 1988; Lynch-Stieglitz et al., 1995). In general, the $\delta^{13}C$ of DIC in the modern ocean is controlled by a combination of air-sea gas exchange, the preformed nutrient content of waters, and the respiration of particulate organic matter at depth (Broecker & Maier-Reimer, 1992; Curry et al., 1988; Lynch-Stieglitz et al., 1995). On glacial-interglacial timescales, the $\delta^{13}C$ of DIC is influenced by CO_2 exchange with the atmosphere, the export of isotopically light carbon from the surface ocean to the deep ocean (i.e., the biological pump), and the formation and dissolution of calcium carbonate. In the Southern Ocean, however, $\delta^{13}C$ is primarily used as a tracer for CO_2 exchange between the atmosphere and water masses formed near Antarctica owing to the dominant role of air-sea CO_2 exchange (Lynch-Stieglitz et al., 1995). Accordingly, the relatively enriched $\delta^{13}C$ of SAMW and AAIW reflects CO_2 exchange between the ocean and atmosphere (Charles et al., 1993; Lynch-Stieglitz et al., 1994), whereas depleted $\delta^{13}C$ of AABW records the accumulation of respired CO_2 at depth and isolation from the atmosphere (Curry et al., 1988; Mackensen et al., 1993). The oxygen isotopic composition of benthic foraminiferal calcite ($\delta^{18}O$) is influenced by the temperature effects on isotopic fractionation in calcite and the $\delta^{18}O$ of seawater ($\delta^{18}O_{sw}$), the latter of which is determined by salinity, advection, and global ice volume (Adkins, 2013; LeGrande & Schmidt, 2006). Once isolated from the surface, the $\delta^{18}O$ signature of exported water masses is conservative and can only be altered via mixing; therefore, $\delta^{18}O$ can be used to examine changes in ocean circulation and the key physical parameters that influence ocean structure (Adkins, 2013; Lund et al., 2015; Sikes, Elmore, et al., 2016).

1.2. Paleoceanographic Reconstructions in the Southern Ocean

The ocean's vertical structure and circulation are thought to have been different during the LGM (Figure 2). Enriched pore water chlorinity (a proxy for salinity) and $\delta^{18}O_{sw}$ indicate that the deep glacial Southern Ocean was both colder and saltier (Adkins et al., 2002; Schrag et al., 2002). This has been interpreted as a more stratified ocean than today owing to a combination of influences from colder atmospheric temperatures, expanded sea ice, and enhanced brine rejection. Expanded, permanent sea ice would have broadened the region of buoyancy loss in the Southern Ocean and shifted the locus of meltwater delivery north, likely having a strong influence in defining the ocean's salinity structure. This would have favored the formation of denser southern-sourced waters and reconfigured the geometry of Southern Ocean overturning as the isopycnal boundary shoaled (Abernathey et al., 2016; Bostock et al., 2004; Ferrari et al., 2014; Keeling & Stephens, 2001; Sigman et al., 2010; Sikes, Elmore, et al., 2016; Watson et al., 2015). Similarly, reduced seasonal sea ice would have minimized the freshwater input required for modern AAIW production, which could have manifested in a denser glacial AAIW during the LGM (Keeling & Stephens, 2001; Pahnke & Zahn, 2005).

Northern-sourced interior waters from the Atlantic shoaled during the LGM to form Glacial North Atlantic Intermediate Water (GNAIW; e.g., Curry & Oppo, 2005; Gherardi et al., 2009; Lund et al., 2015). Today, geostrophic constraints restrict water shallower than the Drake Passage sill depth from entering the Southern Ocean and contributing to southern-sourced deep water production (Talley, 2013). GNAIW was not deep enough to flow southward into the Southern Ocean because a net meridional geostrophic transport cannot be supported in the absence of a net zonal circumpolar pressure gradient above the sill depth (Sikes et al.,

2017). The comparison of depth transects from the southwest Atlantic and Pacific demonstrated that the deep Pacific and Atlantic oceans were more distinct from one another during the LGM in both $\delta^{13}C$ and $\delta^{18}O$, attributable to the inability of GNAIW to enter the Southern Ocean (Sikes et al., 2017). As a result, the *Deep Gateway* hypothesis suggests that southern-sourced deep waters lacked an Atlantic component and were instead composed primarily of denser Pacific- and Indian-sourced deep waters (Figure 2).

Colder atmospheric temperatures and stronger meridional thermal gradients during the LGM likely prompted an equatorward shift in the frontal location of the SHW and reduced the upwelling of CO_2-rich waters in the Southern Ocean (Toggweiler, 2009; Toggweiler et al., 2006). A broader region of negative buoyancy, coupled with an equatorward shift in the westerlies, would have enhanced the formation of denser interior waters and restricted air-sea CO_2 exchange. Indeed, old radiocarbon ages in the deep southwest Pacific Ocean support reduced ventilation and overturning rates compared to the Holocene (Ronge et al., 2016; Sikes, Cook, et al., 2016; Sikes et al., 2000; Skinner et al., 2015, 2017). Less constrained are the structural and CO_2 storage changes at intermediate depths in this region, as evidenced by two prevailing hypotheses that put forth conflicting glacial changes to AAIW. Pahnke and Zahn (2005) observed depleted $\delta^{13}C$ in core MD97-2120 (1,200 m) during the LGM and suggested that enhanced sea-ice extent during the LGM had two main effects on AAIW ventilation and structure. First, a sea-ice cap would have prevented air-sea CO_2 exchange during AAIW formation. Second, the region of buoyancy gain shifted north and cut off the freshwater supply needed to form AAIW resembling its modern configuration, which is in agreement with modeling of a saltier glacial AAIW (Keeling and Stephens, 2001). Regionally depleted $\delta^{13}C$ and low carbonate ion concentrations ($[CO_3^{2-}]$) at intermediate depths during the LGM support poorly ventilated intermediate waters in the southwest Pacific (Bostock et al., 2004; Elmore et al., 2015; Sikes, Elmore, et al., 2016) (Figures S2 and S4). Another study invokes a similar mechanism whereby the region of positive buoyancy shifting north during the LGM, but instead suggest that this freshened and shoaled AAIW, which increased CO_2 storage in an isolated deep ocean (Ronge et al., 2015).

After the LGM, Antarctic ice core records indicate that the steady rise in atmospheric CO_2 was punctuated by two rapid phases during Heinrich Stadial 1 (Marcott et al., 2014). Among the mechanisms proposed to explain the transfer of CO_2 from the ocean interior to the atmosphere are a poleward shift in the westerlies, reduced sea-ice extent, and, more recently, changes in the vertical structure of the Southern Ocean. A poleward shift in the westerlies is thought to have reinvigorated Southern Ocean upwelling (Allen et al., 2015; Anderson et al., 2009; Sikes, Elmore, et al., 2016; Sikes et al., 2009; Toggweiler, 2009, for a summary, see Denton et al., 2010), while reduced sea-ice extent may have allowed for equilibration between the ocean interior and atmosphere (Stephens & Keeling, 2000). Globally asynchronous benthic $\delta^{18}O$ depletion at the end of the LGM suggests that deglacial changes in ocean structure and circulation were basin-specific and time transgressive (Stern & Lisiecki, 2014), highlighting the importance of constraining the extent to which changes in the Southern Ocean's vertical structure contributed to the rapid release of CO_2 from the ocean interior after the LGM. A sediment core depth transect from the southwest Pacific indicates that there was an early onset in $\delta^{18}O$ depletion at intermediate depths (<1,600 m) during Heinrich Stadial 1 (HS1), while the arrival of this signal in the deeper ocean occurred after HS1 (Sikes et al., 2017; Sikes, Elmore, et al., 2016). Indeed, benthic $\delta^{13}C$ below 1,600 m during HS1 only became slightly enriched while the greatest enrichment occured at intermediate depths (Sikes, Elmore, et al., 2016). Sikes et al. (2017) and others (Bostock et al., 2004; Bova et al., 2015; Pahnke & Zahn, 2005; Sikes, Cook, et al., 2016; Sikes, Elmore, et al., 2016) interpret enriched intermediate water $\delta^{13}C$ during HS1, relative to the LGM, as the release of CO_2 from these depths due to a poleward displacement of the SHW, causing the two-step rise in atmospheric CO_2 across this interval. In contrast, although converging neodymium isotopes in deep South Pacific cores (>3,000 m) are interpreted as evidence of mixing and destratification—thereby releasing CO_2 from the deep ocean—the mechanism relies on deep ocean warming (Basak et al., 2018). Regional temperature reconstructions indicate that warming of the deep Pacific lagged the initial glacial termination and CO_2 rise (Elderfield et al., 2012; Skinner & Shackleton, 2005).

1.3. This Study

While a number of mechanisms have been proposed to explain the deglacial rise in atmospheric CO_2, the role of the Pacific Ocean is unresolved. There is recent evidence for both top-down structural forcing of

CO_2 ventilation (e.g., Sikes et al., 2017) and bottom-up forcing (e.g., Basak et al., 2018; Du et al., 2018). Thus, the deglacial structural changes that may have influenced the release of CO_2 from this region, and from what depths CO_2 was released from, remain uncertain. This work examines how structural changes in southwest Pacific waters document contributions from Southern Ocean overturning circulation and carbon storage to glacial and deglacial climate change.

2. Methods

2.1. Core Materials and Stratigraphy

Calculated vertical benthic isotope differences using *Cibicidoides spp*. stable isotope data are based on a composite depth transect of jumbo piston cores (JPC) and gravity cores (GC) taken from the Tasman Sea and New Zealand's Hawke's Bay and Bay of Plenty in the southwest Pacific Ocean (Figure 1a). Cores from this depth transect are currently bathed by SAMW, AAIW, and AABW, which are exported from the Southern Ocean, CDW, and the return flow of PDW (Hanawa & Talley, 2001; Piola & Georgi, 1982; Sloyan & Rintoul, 2001, Figures 1b and S1). Their high sedimentation rates allow for a high-resolution examination of the southwest Pacific Ocean since the last glaciation. These isotope data were previously compiled and archived under Sikes, Elmore, et al. (2016, see Figure S2); the same cores are used here to provide data on all major water masses from 660 to 3,800 m (Figure 1b and Table S1). Stratigraphy for the New Zealand cores was generated from tephra-controlled age models (Shane et al., 2006) based on radiocarbon (Sikes & Guilderson, 2016). The proximity of the New Zealand cores to terrestrial volcanoes generated multiple tephra layers in the Bay of Plenty cores, while the Hawke's Bay core contained one tephra and was coupled with planktic oxygen isotopes to generate complete stratigraphy (Sikes, Elmore, et al., 2016). In the Tasman Sea cores, ^{14}C-AMS dating on planktic foraminifers was converted to calendar ages using IntCal13 (Marine 13), which incorporates a surface reservoir age correction of 400 years (Reimer et al., 2013; Sikes, Elmore, et al., 2016, see Text S1). The high-resolution benthic isotope records published in Sikes, Elmore, et al. (2016, Figure S2) were used here to calculate the relative differences in geochemical composition between ocean depths since the last glaciation, ~23.0–18.0 thousand years ago (ka).

2.2. Vertical Isotope Difference Calculations

This work focuses on changes in southwest Pacific Ocean water column structure and CO_2 storage since the LGM. Rather than identifying maximum isotope gradients across a depth transect as a means to locate geochemical boundaries between the LGM and Holocene (e.g., Lund et al., 2011), we use calculations of vertical benthic isotope differences to provide details on the relative changes in isotopic composition between depths, independent of glacial-interglacial changes in the overall isotopic signal. The use of benthic isotope differences provides insight on processes likely occurring during the wintertime conversion of water masses in the Southern Ocean as opposed to planktic-benthic isotope differences, which could be influenced by seasonality.

We assessed the CO_2 content of subsurface water masses relative to the atmosphere using $\delta^{13}C$ as a proxy. The $\delta^{13}C$ from our shallowest core (RR0503-87JPC; 663 m), which sits at SAMW depths today (Figures 1b and S1), has had a consistent difference with the atmospheric $\delta^{13}C$ signal (Schmitt et al., 2012) since the LGM, suggesting that SAMW remained in the same isotopic equilibrium with the atmosphere during the LGM and across the deglaciation (Figure S3). This is consistent with mode and shallow intermediate water radiocarbon records from the southwest Pacific (Rose et al., 2010; Sikes, Cook, et al., 2016). Consequently, we use 87JPC as a well-ventilated end-member for $\Delta\delta^{13}C$ ($\Delta\delta^{13}C = \delta^{13}C_{shallowest\_cib} - \delta^{13}C_{deep\_cib}$) calculations between 660 m and all deeper cores in this transect. Similar steps were taken to generate records of vertical oxygen isotope differences to observe relative changes in water column structure between 660 m and depths down to 3,800 m. While $\delta^{18}O$ is largely driven by the global ice volume signal on glacial-interglacial timescales (Figure S2), this signal is time transgressive (e.g., Skinner & Shackleton, 2005; Stern & Lisiecki, 2014). Calculating the $\Delta\delta^{18}O$ ($\Delta\delta^{18}O = \delta^{18}O_{shallowest\_cib} - \delta^{18}O_{deep\_cib}$) distinguishes the regional signal from the global signal and illuminates time transgressive differences in $\delta^{18}O$ with depth.

$\Delta\delta^{18}O$ and $\Delta\delta^{13}C$ for depths between 660 and 3,800 m (Figures 3a and 3b) were calculated by first resampling to a common timescale by optimal interpolation to a resolution of 100 years. For each core, $\delta^{13}C$ and $\delta^{18}O$ were then differenced from that of the shallowest core (87JPC). Other studies from this region

relied on the use of infaunal benthic species in the absence of *Cibicidoides spp*. to produce regional stable isotope records (Pahnke & Zahn, 2005; Ronge et al., 2015); this precluded us from including calculated $\Delta\delta^{18}O$ between our SAMW core (*Cibicidoides*-based) and these cores (see Figure S4). Because isotope records in this analysis lack centennial-scale resolution, we applied a 10-point filter to these differences to remove high-pass information and examine millennial-scale changes in carbon storage and water column structure since the LGM. Isotope differences were visualized with contour plots in MATLAB (Figures 3c and 3d). A color spectrum was assigned to the full range of calculated values for the $\Delta\delta^{18}O$ and $\Delta\delta^{13}C$ records (Figures 3c and 3d; also see Text S2). Time slices for millennial-scale events (Figure 4) were also generated by averaging the $\Delta\delta^{18}O$ and $\Delta\delta^{13}C$ from each depth for the following time intervals: LGM (23.0–18.0 ka), HS1 (17.5–14.5 ka), the Antarctic Cold Reversal (ACR; 14.5–12.9 ka), Younger Dryas (YD; 12.8–11.0 ka), and Holocene (10.5–0 ka).

3. Results

3.1. $\Delta\delta^{18}O$ Reconstructions

During the LGM, the range in $\Delta\delta^{18}O$ among the water masses was smaller than the modern ocean (Figure 3a). The $\Delta\delta^{18}O$ between waters at 660 and 1,100 m at the end of the LGM was ~0.6‰, while the $\Delta\delta^{18}O$ from 1,100 to 3,800 m was only ~0.3–0.5‰; this was less than that seen between the shallowest two cores (Figure 3a). The $\Delta\delta^{18}O$ between 1,100 and 1,600 m was ~0.2‰. The large difference between 660 and 1,100 m suggests strong stratification, and the similarity between 1,100 m and depths down to 3,800 m indicates a more uniform water column below 1,100-m depth (Figure 3c). In contrast, the early Holocene had a ~0.2‰ difference between 660 and 1,100 m, and a 1.0‰ range between 1,600 and 3,800 m.

During HS1, there were rapid increases in $\Delta\delta^{18}O$ across parts of the depth transect. The large increase in $\Delta\delta^{18}O$ of ~0.3–0.6‰ seen at deeper layers (Figure 3a) was driven by the earlier deglacial $\delta^{18}O$ shift in the 660-m reference core, in concert with the AAIW-depth1,100-m core, at ~17.0 ka (Figure S2). In contrast, the deglacial $\delta^{18}O$ shift in deeper cores did not start until the second half of HS1 (Figure S2). A greater contrast in $\Delta\delta^{18}O$ between deeper intermediate waters (those at 1,600 m) and those below 2,500 m can be seen by the second half of HS1 (Figure 3c). The result was that waters at 3,800 m were most dissimilar to SAMW at the end of HS1 than any time before or after, and the $\delta^{18}O$ of water between 2,000 and 3,800 m was more dissimilar than any previous time (Figures 3a and 3c).

At the start of the ACR (14.5 ka), the $\Delta\delta^{18}O$ trend between SAMW and the deeper cores reverses, with the $\Delta\delta^{18}O$ of deeper cores diminishing. The three cores above 2,500 m became more similar to one another as the $\Delta\delta^{18}O$ at these depths again resembled their relative differences at the LGM (Figure 3a). This change was caused by increased pace in the deglacial $\delta^{18}O$ shift in the 1,100, 1,600, and 2,000 m cores relative to the SAMW core (Figure S2). In contrast, the $\Delta\delta^{18}O$ of waters below 2,500 m, which had similar differences at the end of HS1, became more similar to SAMW across the ACR owing to a slower pace of $\delta^{18}O$ depletion (Figure S2). As a result, $\Delta\delta^{18}O$ in the upper water column between 660 and 2,000 m became most similar by the end of the ACR (Figure 3a). $\Delta\delta^{18}O$ values below mid-depth remained stable during the ACR (Figure 3a), indicating the rate of $\delta^{18}O$ change at these depths mostly kept pace with SAMW (Figure S2). The exception to this deep core trend was core Z2112 at 2,858 m, which showed a significant decrease in $\Delta\delta^{18}O$ across the ACR, becoming similar to the 1,600-m core by the YD (Figure 3a).

In the early Holocene (10.5–8.0 ka), the most notable change is the increase in $\Delta\delta^{18}O$ between 660- and the 1,100- and 1,600-m cores immediately following the YD (Figure 3a). This once again places the largest $\Delta\delta^{18}O$ contrast between SAMW and intermediate-depth waters. Concurrently, the contrast with waters at 2,500 to 2,800 m diminishes (Figure 3a). This trend reverses at 8.0–6.0 ka with the $\Delta\delta^{18}O$ of all water above 3,000 m becoming more similar to SAMW. $\Delta\delta^{18}O$ in water at 3,300 m became more different than SAMW after the YD, whereas it became more similar in waters at 3,800 m (Figure 3a).

3.2. $\Delta\delta^{13}C$ Reconstructions

During the LGM, the range in shallow-to-deep $\Delta\delta^{13}C$ between 1100 and 3800 m (~1.0‰) was nearly twice the magnitude of the Holocene (~0.5‰, Figure 3b). This is in contrast to the range in water column $\Delta\delta^{18}O$, which was at a minimum during the LGM (Figure 3a). The $\Delta\delta^{13}C$ between 660 and 1,100 m

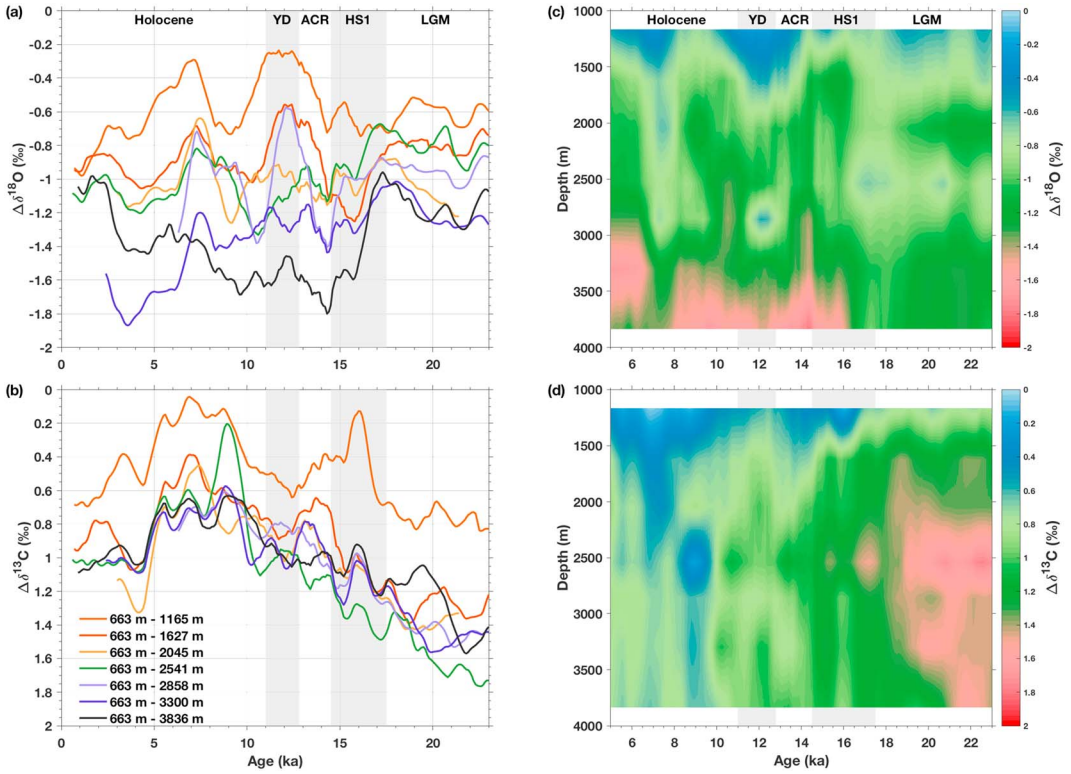

Figure 3. Calculated vertical isotope differences. (a) Vertical oxygen isotope differences ($\Delta\delta^{18}O$) calculated between the 660 m SAMW core and depths down to 3,800 m. (b) Vertical carbon isotope differences ($\Delta\delta^{13}C$) calculated for the same depths. (See Text S2 for details on contouring.) (c) $\Delta\delta^{18}O$ contoured to depth and (d) $\Delta\delta^{13}C$ contoured to depth. For Figures 3c and 3d, a three-color spectrum was assigned to the full range of $\Delta\delta^{18}O$ and $\Delta\delta^{13}C$ values; isotopically distinct waters are shaded green and red, while isotopically similar waters are shaded blue. In Figures 3a and 3b, millennial-scale intervals are labeled, and the deglacial warm periods (HS1 and YD) are shaded gray. For these vertical difference calculations, $\Delta\delta^{18}O$ and $\Delta\delta^{13}C$ of zero denote that the isotopic composition is the same between the SAMW reference core and any other depth.

(~0.8‰) was nearly the same magnitude as the range in $\Delta\delta^{13}C$ for waters between 1,100 and 3,800 m (Figure 3b). The depth of this strong $\Delta\delta^{13}C$ gradient between SAMW and 1,100 m coincided with a large $\Delta\delta^{18}O$ across the same depths (Figure 3a), placing the depth of greatest geochemical contrast between 660 and 1,100 m. The $\Delta\delta^{13}C$ difference between 1,100 and 1,600 m (~0.6‰) was nearly as large as the range in $\Delta\delta^{13}C$ among depths at or below 1,600 m; this is in contrast to the $\Delta\delta^{18}O$, which was ~0.2‰ between 1,100 and 1,600 m. Plotting $\Delta\delta^{13}C$ with depth highlights a mid-depth $\Delta\delta^{13}C$ maximum at 2,500 m of ~1.8‰ (Figure 3d), indicating the $\delta^{13}C$ of the mid-depth southwest Pacific was more dissimilar to SAMW at the LGM than were the bottom waters.

Across the deglaciation, the $\Delta\delta^{13}C$ below 1,600 m steadily became more similar to SAMW (Figure 3b). Waters at 1,100 and 1,600 m also had decreases in $\Delta\delta^{13}C$, but this occurred in two abrupt steps. At 16.5 ka, ~1.0 ka after the onset of HS1, there was a rapid reduction in $\Delta\delta^{13}C$ to almost zero between SAMW and 1,100 m (Figure 3b), which was largely driven by a ~0.5‰ $\delta^{13}C$ enrichment in the 1,100-m core (Figure S2). At the same time, a ~0.25‰ $\delta^{13}C$ depletion in the SAMW core was responsible for a small reduction in $\Delta\delta^{13}C$ in the deeper cores (Figures 3b and S2). When plotted with depth, it is evident that the steepest difference in $\delta^{13}C$ moves from waters between SAMW and AAIW to depths deeper than these cores (Figure 3d). Near the end of HS1 (~15.5 ka), waters at 1,600 m abruptly became more similar to SAMW and 1,100 m, with the $\Delta\delta^{13}C$ at 1,600 m the smallest since the LGM (Figure 3b). Concurrently, the $\Delta\delta^{13}C$ between SAMW and 1,100 m returned to almost LGM values between the end of HS1 and across the ACR (Figure 3b). The steady, decreasing trend in $\Delta\delta^{13}C$ below 1,600 m caused the water column to be most similar at the ACR-YD transition, with the $\Delta\delta^{13}C$ for all cores falling between 0.6 and 1.0‰ (Figures 3b and 3d).

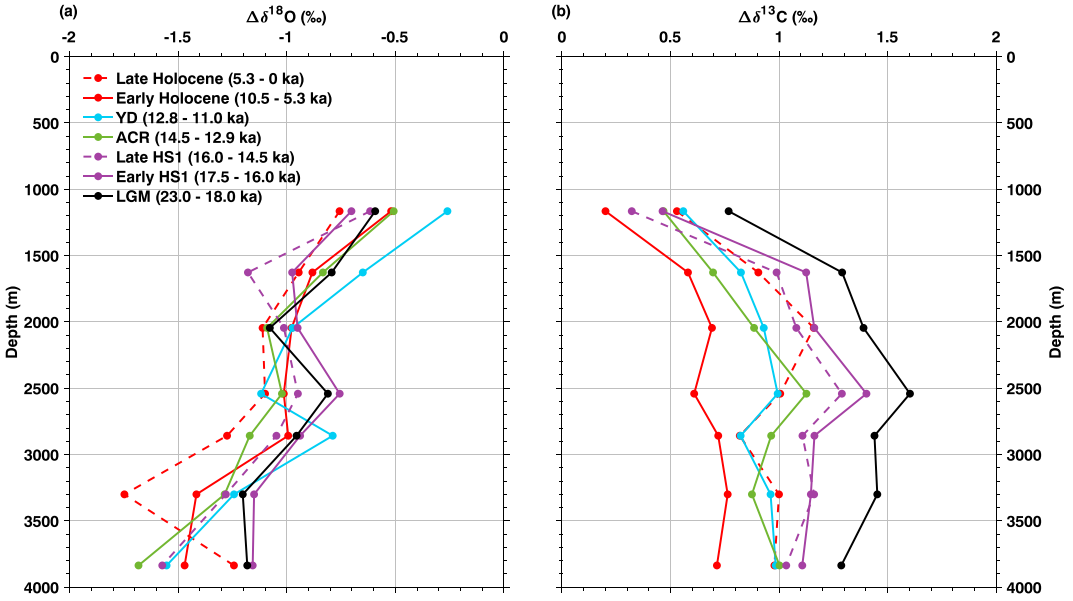

Figure 4. Time-averaged vertical difference slices. $\Delta\delta^{18}O$ (a) and $\Delta\delta^{13}C$ (b). Vertical differences for both isotopes were averaged for the Last Glacial Maximum (LGM), the Holocene, and millennial-scale climate intervals: Heinrich Stadial 1 (HS1), Antarctic Cold Reversal (ACR), and Younger Dryas (YD); age ranges for these intervals are denoted in the figure legend. Large changes in $\Delta\delta^{18}O$ and $\Delta\delta^{13}C$ above 2,000 m occurred simultaneously during the early HS1 while $\Delta\delta^{18}O$ between 2,500 and 3,800 m did not change between the LGM and early HS1, suggesting deep ocean stratification persisted well after the deglacial onset. Enhanced $\Delta\delta^{18}O$ at 1,600 m during HS1 suggests that these depths were shielded from sea-ice driven buoyancy changes that helped convert CO_2-rich GAAIW to well-ventilated AAIW during HS1. $\Delta\delta^{13}C$ below 2,000 m remained enhanced relative to depths above this until after the YD. The step change in $\Delta\delta^{13}C$ below 1,600 m between the LGM and HS1 occurred without noticeable changes in structure, suggesting CO_2 was slowly ventilated from the deep Pacific in the early stages of the deglaciation.

In the early Holocene, AAIW again became more similar to SAMW while the $\Delta\delta^{13}C$ between SAMW and deeper waters continued to decrease (Figures 3b and 3d). There were also rapid and significant reductions in $\Delta\delta^{13}C$ between SAMW and the 2,500-m core centered on 9.0 ka, for which the $\Delta\delta^{13}C$ reduced by ~1.0‰ (Figure 3b). In the late Holocene, the $\Delta\delta^{13}C$ across all depths appears to increase after 5.0 ka (Figure 3b). This is a direct result of a ~0.5‰ increase in the $\delta^{13}C$ values in the 660-m core rather than changes in the $\delta^{13}C$ of the deeper cores (Figure S2). We have no clear oceanographic explanation for this particular $\delta^{13}C$ increase.

4. Discussion

The $\delta^{18}O$-independent stratigraphy in this depth transect of high-resolution cores allowed us to use the calculated $\Delta\delta^{18}O$ to identify millennial-scale changes in water mass structure since the LGM without having to rely on low-resolution sea level curves to remove the global ice volume signal (e.g., Elderfield et al., 2012; Roberts et al., 2016; Rohling & Bigg, 1998; Rohling et al., 2014) of 1.1–1.3‰ (Adkins et al., 2002; Fairbanks, 1989). The $\Delta\delta^{18}O$ among these cores should therefore reflect changes in the salinity component of $\delta^{18}O_{sw}$ and water mass temperature across depths in the region, relative to SAMW. Time-slice averaged $\Delta\delta^{18}O$ for millennial-scale climate events is useful to highlight the timing of regional changes between depths during the deglaciation that are normally masked by the global signal (Figure 4a). Previous work has established that the SAMW CO_2 content in this area has been controlled by exchange with the atmosphere since the LGM (Lynch-Stieglitz et al., 1994; Rose et al., 2010; Sikes, Cook, et al., 2016), making the $\delta^{13}C$ in our shallowest core at SAMW depth a workable proxy for an atmospheric endmember (Figure S3).

4.1. The Last Glacial Maximum

Two components of the glacial $\Delta\delta^{18}O$ suggest that the vertical structure of the southwest Pacific Ocean was different during the LGM relative to the Holocene. First, enhanced $\Delta\delta^{18}O$ between 660 and 1,100 m, with reduced $\Delta\delta^{18}O$ between 1,100 and 3,800 m, reveals that the locus of stratification shoaled to at least 1,100 m in the southwest Pacific and that glacial SAMW and *glacial AAIW* (GAAIW) were more distinct from one another (Figures 3a, 3c and 4a). Second, the range in $\Delta\delta^{18}O$ between 1,100 and 1,600 m was the smallest at the end of the LGM than at any time until the Holocene (Figure 3a), further indicating that GAAIW occupied waters below the locus of stratification during the LGM and was likely both saltier and less ventilated (Figures 2 and S5). This is in contrast to today, whereby the southwest Pacific at 1,100 m is occupied by the core of a relatively fresh and well-ventilated AAIW that is formed north of the PF and is distinct in its salinity from the PDW below it (Figure 1b). Currently, AAIW formation is reliant on freshening from the seasonal production of sea-ice meltwater (Groeskamp et al., 2016; Saenko et al., 2002; Saenko & Weaver, 2001). During the LGM, however, expansion of permanent winter sea ice broadened the region of negative buoyancy around Antarctica (Benz et al., 2016; Ferry et al., 2015; Watson et al., 2015). Moreover, geostrophic constraints require that the PF could not have shifted north as this front is bound by bathymetry (Toggweiler & Samuels, 1993). We suggest that these changes would have placed the GAAIW formation zone beneath expanded sea ice in a region of negative buoyancy that transitioned toward a region of positive buoyancy at the sea-ice edge (Keeling & Stephens, 2001, Figure 2). Coupled with the glacial ocean having been both colder and saltier during the LGM (e.g., Adkins et al., 2002; Elderfield et al., 2012), formation of AAIW in a zone of enhanced brine rejection would have favored the formation of a denser, saltier GAAIW (Keeling & Stephens, 2001). We infer that a northward shift of the sea ice melting zone to the region of SAMW formation would have caused SAMW to be fresher than GAAIW (Figure S5), enhancing the density and compositional differences between these two water masses as documented by the greater difference in $\delta^{18}O$ (Pahnke & Zahn, 2005, Figures 2 and 3a).

This interpretation appears to contrast with that of Ronge et al. (2015), which inferred a shoaled and fresher GAAIW during the LGM. However, our interpretation of a saltier GAAIW underlying a shallow and much fresher SAMW is consistent if the shallower cores from that study (~940 to 970 m) sat within the boundary between these intermediate water masses. Today, a steep salinity gradient is present above AAIW (Figure 1b); this was also likely the case during the LGM, with the difference between these studies being that we suggest glacial SAMW was the fresher water mass. The depths of our cores compliment those in Ronge et al. (2015) and Pahnke and Zahn (2005), and the suite of cores taken together (Figure S4) suggest that SAMW depths were the locus of freshening during the LGM with the $\delta^{18}O$ below ~900 m becoming more dissimilar from SAMW with depth. These cores also appear to have sat across an increasing $\delta^{13}C$ gradient in the water column (Figure 5).

At the same time, the $\Delta\delta^{18}O$ of glacial waters between 1,100 and 3,800 m was more homogenous than today, with $\delta^{18}O$ values between 1,100 m and 1,600 m and those between 2,000 and 3,000 m being the most similar than at any other time except for a brief period during the late HS1 (Figures 3a and 3c). The small range in $\Delta\delta^{18}O$ between intermediate depths at 1,100 and 1,600 m suggests similar properties, and since brine rejection has a minimal impact on $\delta^{18}O$ (Craig & Gordon, 1965) the diminished $\Delta\delta^{18}O$ between 1,100 and 3,800 m suggests that the entire southwest Pacific water column was occupied by waters with a similar source. The hypothesis that the shoaling of NADW above the Drake Passage sill depth prevented North Atlantic-sourced waters from entering the glacial Southern Ocean requires that PDW fed both the upper and lower branches of the Pacific overturning circulation during the LGM (Sikes et al., 2017). The glacial homogeneity in $\Delta\delta^{18}O$ between 1,100 and 3,800 m supports this idea and suggests that PDW-component CDW was the source of both GAAIW and AABW during the LGM (Figure 2).

The larger $\delta^{13}C$ contrast ($\Delta\delta^{13}C$) between SAMW in our atmosphere proxy core at 660 m and all water masses down to 3,800 m indicates much greater CO_2 storage at depths below our 660-m core during the LGM (Ronge et al., 2016; Sikes, Cook, et al., 2016; Sikes, Elmore, et al., 2016; Skinner et al., 2015, Figures 3b and 4b). To assess the robustness of this signal regionally, we complied the $\Delta\delta^{13}C$ for regional AAIW-depth cores (Bostock et al., 2004; Pahnke & Zahn, 2005; Ronge et al., 2015, Figure 5). The improved vertical resolution highlights a consistent pattern of intermediate-depth $\Delta\delta^{13}C$ to the north, east, and west of New Zealand, and establishes that the greater difference in $\delta^{13}C$ between SAMW and AAIW can be

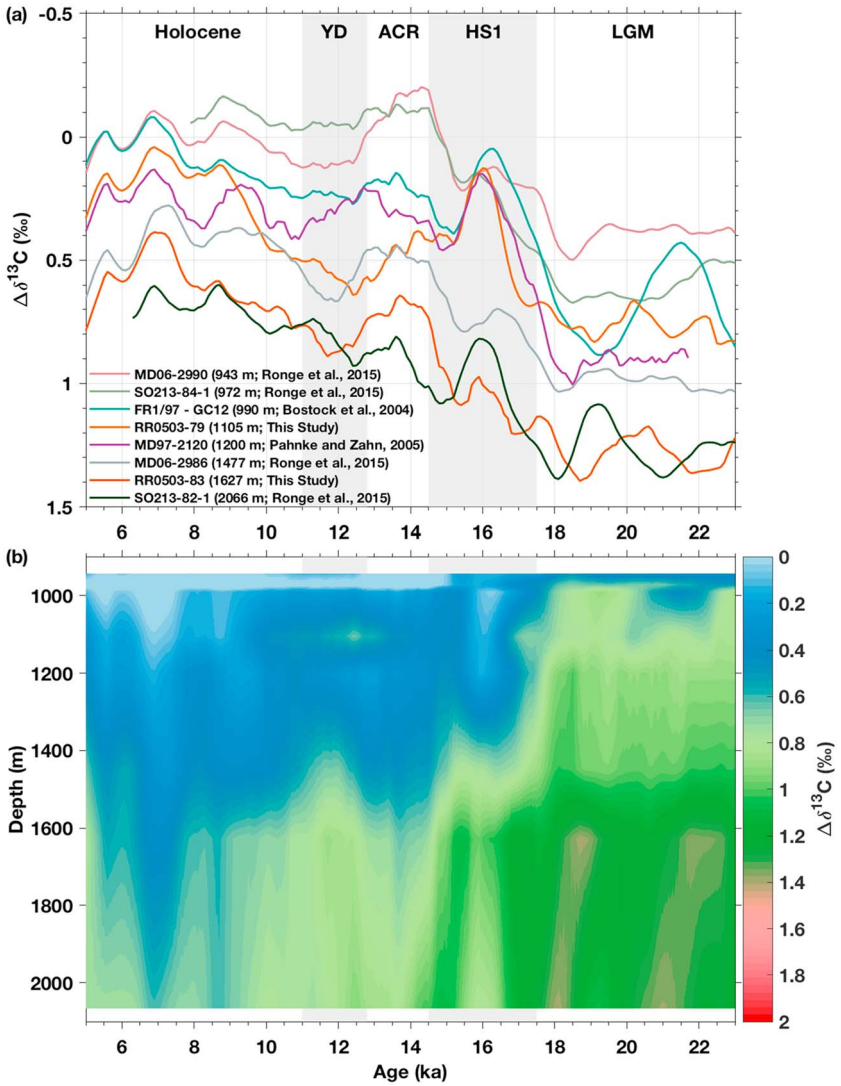

Figure 5. A regional compilation of intermediate- and mid-depth $\Delta\delta^{13}C$. (a) $\Delta\delta^{13}C$ for published records of regional cores at intermediate- and mid-depth around New Zealand—MD06-2990 (943 m, pink), SO213-84-1 (972 m, light green), MD06-2986 (1,477 m, gray), SO213-82-1 (2,066 m, dark green) (Ronge et al., 2015); FR1/97-GC12 (990 m, blue; Bostock et al., 2004); and MD97–2120 (1,200 m, purple; Pahnke & Zahn, 2005)—was calculated for comparison to cores in this study (79JPC and 83JPC). (b) Regional $\Delta\delta^{13}C$ contoured to depth. During the LGM, there is strong coherence in $\Delta\delta^{13}C$ between ~940 and 1,400 m, which is distinct from $\Delta\delta^{13}C$ at 1,600 m and below; this highlights a CO_2-rich GAAIW present in the glacial southwest Pacific Ocean. $\Delta\delta^{13}C$ in MD06-2990 (~940 m) sits slightly above the $\Delta\delta^{13}C$ from other intermediate-depth cores, suggesting it may have sat near the boundary between a well-ventilated SAMW and isolated interior waters. The strong contrast in $\Delta\delta^{13}C$ between GAAIW and the waters below it suggests that these were fundamentally distinct water masses during the LGM, with greater CO_2 storage at intermediate depths, relative to the Holocene, and much greater CO_2 storage in the underlying CDW.

considered representative of intermediate-depth,southern-sourced water masses in the southwest Pacific during the LGM (Figure 5). The enhanced $\Delta\delta^{13}C$ between SAMW and depths below ~ 940 m, relative to the early Holocene, places the regional geochemical divide around or above that depth (Figure 5), consistent with the $\delta^{18}O$ gradient among the same cores (Figure S4). This indicates that GAAIW was more poorly ventilated than today (Pahnke & Zahn, 2005; Sikes, Cook, et al., 2016) and supports our proposition that denser GAAIW formed beneath sea ice, as indicated by our $\Delta\delta^{18}O$ reconstructions (Figures 2, 3a, and 5).

Whereas more homogenous $\Delta\delta^{18}O$ between 1100 m and 3800 m (Figure 3a) suggests a similar source (PDW/CDW), the large contrast in $\Delta\delta^{13}C$ between intermediate-depth cores sitting at or above 1,400 m and those

cores at or below 1,600 m suggests fundamentally different ventilation signals and distinct water mass pathways (Figures 2 and 5). An equatorward shift in the SHW and reduced upwelling farther south in the Southern Ocean (Anderson et al., 2009; Sikes et al., 2009) would have caused SAMW to remain ventilated, while intermediate waters (~ 940 to 1,400 m) were more isolated from the atmosphere, enhancing carbon storage at these shallow depths during the LGM (Pahnke & Zahn, 2005; Sikes, Cook, et al., 2016, Figure 5). Moreover, the expansion of Pacific-sector sea ice by roughly 5° latitude (Benz et al., 2016; Ferry et al., 2015) would have shoaled the overturning isopycnal boundary by ~500 m (Ferrari et al., 2014; Sikes, Elmore, et al., 2016). Our $\Delta\delta^{13}C$ compilation suggests that the overturning isopycnal boundary may have shoaled to at least 1,600 m during the LGM, relative to its modern depth of ~2,000 m, thus further enhancing CO_2 storage below 1,600 m (Ronge et al., 2015; Sikes, Elmore, et al., 2016, Figures 3b and 5). This supports the interpretation of an isolated GAAIW between ~940 to 1,400 m sitting atop an even more CO_2-rich CDW cell (Figure 2). These observations are consistent with records showing reduced radiocarbon levels and $[CO_3^{2-}]$ in southwest Pacific intermediate waters during the LGM (Elmore et al., 2015; Sikes, Cook, et al., 2016), with greatly reduced radiocarbon and $[CO_3^{2-}]$ below those depths (Allen et al., 2015; Ronge et al., 2016; Sikes, Cook, et al., 2016).

The LGM $\Delta\delta^{13}C$ profile had a maximum at ~2,500 m (Figures 3b and 4b), which aligns with the depth of the oldest glacial radiocarbon ages in the southwest Pacific (e.g., Ronge et al., 2016; Sikes, Cook, et al., 2016; Sikes et al., 2000; Skinner et al., 2015). This increase in $\Delta\delta^{13}C$ by up to 1.0‰ identifies the core of PDW southward return flow and the accumulation of respired CO_2 in this water mass (Figure 4b). With greater sea-ice extent and PDW supplying CO_2-rich water to both GAAIW and AABW, this return flow at mid-depth would have upwelled under a broader region of sea ice with limited exchange with the atmosphere where negative buoyancy transitioned northward to relatively positive buoyancy at the sea-ice edge (Figure 2). A CO_2-rich GAAIW cell would have been the northward flowing water mass that interacted adiabatically with southward flowing PDW (De Lavergne et al., 2017). This resulted in a feedback loop that would have enhanced the accumulation of old, CO_2-rich waters in the intersecting layers of the upper and the lower overturning cells, which caused a greater portion of the deep Pacific Ocean to be isolated from the atmosphere (e.g., Jansen, 2017, Figure 2). This mechanism reconciles the mechanisms proposed by Pahnke and Zahn (2005) and Ronge et al. (2015) by identifying that GAAIW, distinct in CO_2 storage from waters above and below it, was present in the glacial southwest Pacific Ocean. The shoaling of the overturning and ventilation boundaries was integral to enhancing carbon storage at all depths below the locus of stratification that separated SAMW from the poorly-ventilated interior. Rather than stronger CDW upwelling, adiabatic interactions between the north flowing GAAIW and PDW return flow at mid-depth, coupled with an expanded and permanent sea-ice cap, manifested in enhanced intermediate-depth $\Delta\delta^{13}C$ during the LGM (Figures 2 and 5).

4.2. The Deglaciation

4.2.1. Heinrich Stadial 1

The use of regional $\delta^{18}O$ stacks has been instrumental in identifying and assessing the asynchronous arrival of the deglacial $\delta^{18}O$ signal in different ocean basins (Stern & Lisiecki, 2014). Nonetheless, the global ice volume component can mask the temperature and $\delta^{18}O_{sw}$-salinity components, which $\Delta\delta^{18}O$ calculations (Figure 3a) can reveal. Beginning at ~17.0 ka, significant $\Delta\delta^{18}O$ differences between SAMW and the depths below 1,100 m were driven by $\delta^{18}O$ depletion in the 660- and 1100-m cores that led the deglacial shift in deeper waters (Figures 3a and S2). Notably, $\Delta\delta^{18}O$ changes for most of HS1 were limited to waters above 2,000 m and at or below 3,800 m, while it was not until the late HS1-ACR transition that $\Delta\delta^{18}O$ between these depths changed by a significant amount (Figure 4a).

Restructuring of the upper 2,000 m during HS1 may have been linked to sea-ice retreat following the glacial termination (e.g., Ferry et al., 2015). An intermediate water temperature records from a nearby core in the Tasman Sea at 1,100 m indicates that AAIW warming beginning at the end of the LGM was abruptly interrupted by a ~1.3 °C cooling across HS1 (Elmore et al., 2015, Figure S5). We used this temperature record (Elmore et al., 2015), a sea level record (Peltier & Fairbanks, 2006), and the Southern Ocean $\delta^{18}O$-salinity relationship of ~0.5‰ psu^{-1} (Adkins et al., 2002) to estimate the change in salinity for our 1,100-m core across HS1 (see Figure S5). We estimate that AAIW freshened by at least 1 psu during the first half of HS1 (Figure S5), which we suggest made it more buoyant and similar to its modern configuration. HS1 was a period of rapid warming in the Southern Hemisphere (Marcott et al., 2014); the melting of LGM-era sea ice

would have injected cold, fresh meltwater to intermediate depths, contributing to the rapid formation and ventilation of intermediate waters at 1,100 m during this time. This is consistent with modern AAIW water mass formation (Groeskamp et al., 2016; Saenko & Weaver, 2001; Santoso & England, 2004) and observations that rapid sea-ice retreat and the delivery of meltwater to intermediate depths are driving the observed AAIW freshening (Haumann et al., 2016). Notably, the $\Delta\delta^{18}O$ between SAMW and 1,600 m, which was most similar to 1,100 m during the LGM, abruptly increased (Figure 3a), indicating that deeper intermediate depths did not experience these changes (Figure 4a). Box model analyses also suggest that sea-ice meltwater can make AAIW too buoyant to sink to depths below 1,100 m (Hain et al., 2014; Keeling & Stephens, 2001).

The fact that average $\Delta\delta^{18}O$ for depths between 2,500 and 3,300 m did not change during the early HS1 relative to the LGM (Figure 4a) indicates deep ocean stratification remained a feature of the southwest Pacific, but deepened to below 2,000 m (Figure 4a). Temperatures and salinities in the deep ocean largely remained unchanged during the early deglaciation (Elderfield et al., 2010; Roberts et al., 2016; Skinner & Shackleton, 2005), explaining the observed coherence in our time-slice average $\Delta\delta^{18}O$ profiles for the LGM and HS1 at these depths (Figure 4a). The exception is $\Delta\delta^{18}O$ at 3,800 m, which increased dramatically after the LGM and suggests that waters at this depth were colder and/or saltier during HS1 relative to SAMW (Figures 3a and 4a). Pacific basin neodymium reconstructions indicate that strong gradients between 3,600 to 4,000 m in the South Pacific (Basak et al., 2018) and between 1,000 and 4,000 m in the North Pacific (Du et al., 2018) broke down across HS1, which the authors attribute to deep ocean warming. With SAMW warming/freshening across HS1, we would expect to see a reduction in the $\Delta\delta^{18}O$ between SAMW and 3,800 m rather than an increase if deep waters warmed as well (Figures 3a and 4a). Instead, enhanced mixing of abyssal waters from reinvigorated deep ocean circulation (with or without a temperature increase), as suggested by proximal sortable silt records (McCave et al., 2008), can reconcile both the enhanced $\Delta\delta^{18}O$ in our 3,800-m core and the breakdown of neodymium gradients across HS1.

During HS1, our $\Delta\delta^{13}C$ has two distinct ventilation signals in the shallow parts of the depth transect. An abrupt ~0.6‰ reduction starting at 17.0 ka brought the difference between SAMW $\delta^{13}C$ and AAIW at 1,100 m near zero at 16.5 ka, returning to near LGM values by 15.5 ka (Figure 3b). This coincided with the first pulse of rapid atmospheric CO_2 rise during HS1 and enhanced $\Delta\delta^{18}O$ between SAMW and 1,600 m (Figures 3a, 3b, and 6). This was followed at ~15.5–14.5 ka when waters at 1,600 m became abruptly enriched in $\delta^{13}C$, reducing the $\Delta\delta^{13}C$ by ~0.5‰ (Figures 3b and S2). This coincided with the second pulse of rapid atmospheric CO_2 rise during HS1 (Marcott et al., 2014, Figure 6), increased southwest Pacific [CO_3^{2-}] (Allen et al., 2015), and reduced $\Delta\delta^{18}O$ between SAMW and 1,600 m in the latter half of HS1 (Figure 3a and 3b). These observations are consistent with abrupt $\Delta\delta^{13}C$ reduction at AAIW depths in the southwest Pacific (Bostock et al., 2004; Pahnke & Zahn, 2005; Ronge et al., 2015; Sikes, Elmore, et al., 2016, Figure 5) and reduced $\Delta\delta^{13}C_{planktic\text{-}benthic}$ at 1,500 m in the SE Pacific (Siani et al., 2013). Collectively, this suggests the progressive loss of CO_2 from increasingly deeper intermediate layers of the South Pacific, attributable to enhanced AAIW buoyancy, a poleward shift in the westerlies (Anderson et al., 2009; Sikes et al., 2009; Toggweiler & Lea, 2010), and sea-ice retreat (Ferry et al., 2015), the latter of which acted to deepen the upwelling boundary across HS1 (Ferrari et al., 2014).

The $\Delta\delta^{13}C$ below 1,600 m remained enhanced in the early stages of the deglaciation, with a maximum at 2,500 m, but was reduced relative to the LGM (Figures 3b and 4b). For these depths, a slow, steady, and early decrease in $\Delta\delta^{13}C$ suggests that there was initially high CO_2 content at these depths and a progressive decrease in the CO_2 content across HS1 and into the YD (Figures 3b and 4b), an interpretation that is supported by regional radiocarbon records (e.g., Ronge et al., 2016; Sikes, Cook, et al., 2016). It is worth noting that the oscillatory $\Delta\delta^{13}C$ variability overprinting the overall gradual $\Delta\delta^{13}C$ reduction (Figure 3b) is a function of rapid $\delta^{13}C$ variability in the SAMW core (Figure S2). The steady $\Delta\delta^{13}C$ decrease below 1,600 m kept pace with the slow, steady rise in atmospheric CO_2 (Figure 6), suggesting that CO_2 ventilation from deeper depths across the deglaciation provided a background increase against the rapid release of CO_2 from intermediate depths (Figure 6).

This reanalysis suggests a somewhat different scenario than studies that invoke the deep Pacific Ocean as the direct source of CO_2 during HS1 (e.g., Basak et al., 2018; Burke et al., 2015; Du et al., 2018; Ronge et al., 2016).

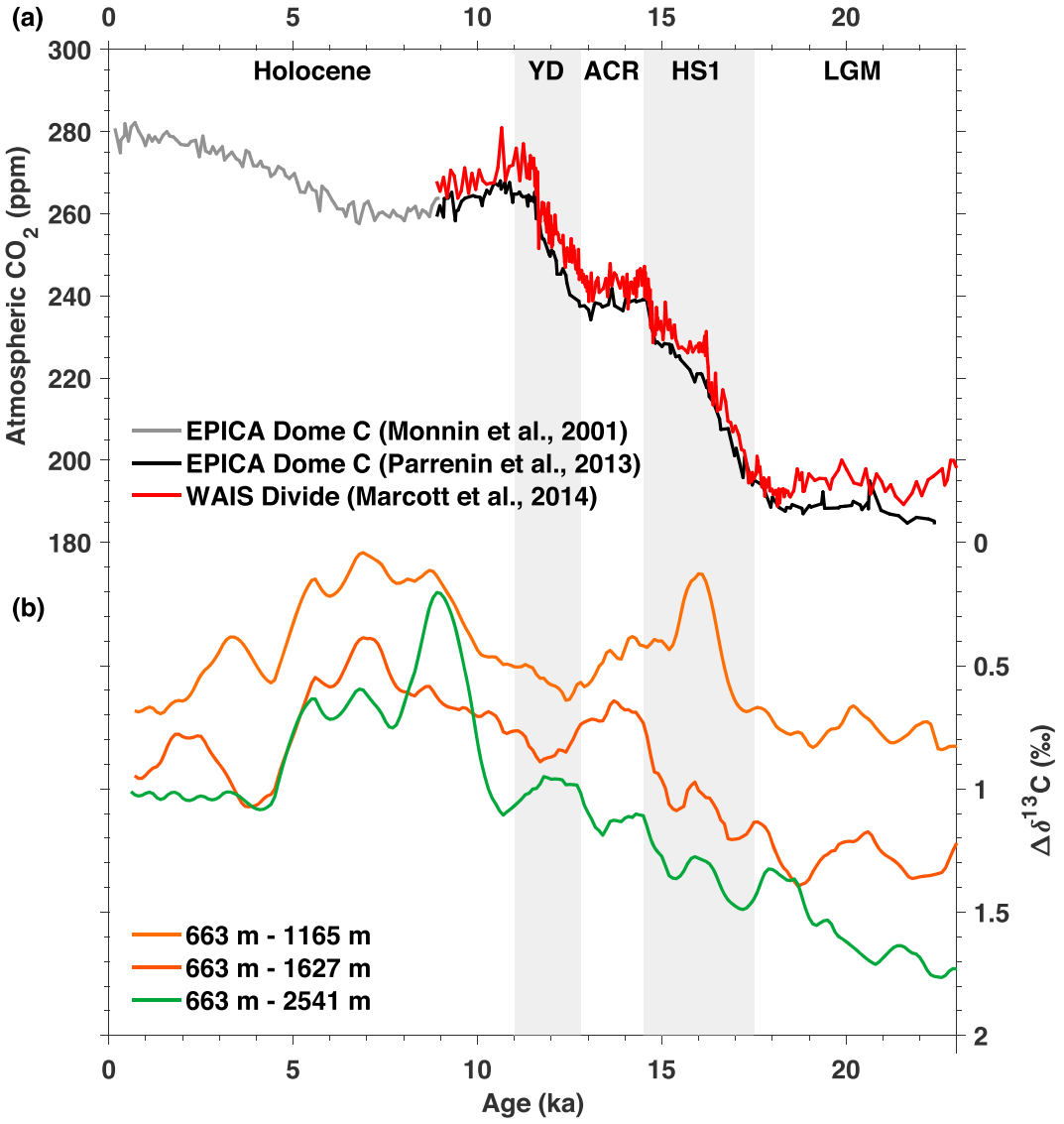

Figure 6. Southwest Pacific $\Delta\delta^{13}C$ and atmospheric CO_2. (a) Atmospheric CO_2 concentrations derived from Antarctic ice core records (Marcott et al., 2014; Monnin et al., 2001; Parrenin et al., 2013). (b) $\Delta\delta^{13}C$ from our depth transect for 1,100, 1,600, and 2,500 m. During HS1, an abrupt reduction in $\Delta\delta^{13}C$ at 1,100 m (b) coincided with the first abrupt rise in atmospheric CO_2 at ~16.5 ka (a) and evidence for reinvigorated Southern Ocean upwelling (Anderson et al., 2009). In the second half of HS1, an abrupt reduction in $\Delta\delta^{13}C$ at 1,600 m coincided with the rapid rise in atmospheric CO_2 at ~15.5 ka. Abrupt reductions in $\Delta\delta^{13}C$ below 2,000 m occurred after the atmospheric CO_2 rise during and after the YD (b). The intermediate $\Delta\delta^{13}C$ suggests that the intermediated-depth southwest Pacific was a key source of CO_2 during HS1. Steady reductions in deep water $\Delta\delta^{13}C$ suggest these depths contributed to the slow deglacial CO_2 rise beginning at the end of the LGM.

The $\Delta\delta^{13}C$ maxima between SAMW and 2,500 m persisted until after the second half of the deglaciation, consistent with South Pacific mid-depth radiocarbon records showing old ages until ~15.0 ka (Ronge et al., 2016; Sikes, Cook, et al., 2016). The patterns we observe are more consistent with the slow loss of CO_2 from the deep ocean via a secondary mid-depth PDW return flow rather than direct equilibration and rapid CO_2 exchange with the atmosphere from the deepest layers, which would have had to occur in the southernmost regions of the Southern Ocean. These regions remained ice covered during HS1 (Wolff et al., 2006). We suggest that upwelled portions of PDW became entrained in an invigorated, north flowing AAIW, allowing some of its CO_2 to ventilate via an intermediate pathway and thereby reducing the $\Delta\delta^{13}C$ from 1,600 through 2,500 m (Figure 4b). Concurrently, the portion of PDW that upwelled

farther south returned north as AABW, having not fully equilibrated with the atmosphere, continuously feeding the mid-depth Pacific Ocean carbon reservoir during HS1 and the early deglaciation (Figure 2b). This interpretation is supported by the fact that $\Delta\delta^{13}C$ in our deeper cores remained persistently greater than those at shallower mid-depths (Figure 4b). Recent model work supports this interpretation, suggesting that both rapid and gradual CO_2 sources are required to account for temporally distinct (i.e., millennial- and centennial-scale) atmospheric CO_2 increases during the deglaciation (Menviel et al., 2018). Our results clarify that CO_2 was released via different mechanisms and from different water depths in the Pacific Ocean after the LGM.

4.2.2. Antarctic Cold Reversal, Younger Dryas, and the Holocene

Across the ACR-YD transition, the $\Delta\delta^{18}O$ in the upper 1,600 m of the southwest Pacific Ocean approached zero (Figure 4a). These intermediate water $\Delta\delta^{18}O$ changes coincided with the deglacial meltwater pulse event (Fairbanks et al., 1992; Weber et al., 2014), suggesting that the homogenization of the signal may have been driven by meltwater-infused, $\delta^{18}O$-depleted water from the Atlantic Ocean as it reentered the Pacific Ocean at intermediate depths (Sikes et al., 2017). While the advance of Antarctic sea ice (Ferry et al., 2015) and Southern Hemisphere glaciers (Garcia et al., 2012; Putnam et al., 2010) during the ACR is indicative of an equatorward shift in the STF across this interval, the STF appears to have remained far enough south to allow Atlantic waters to enter the Indian and Pacific Oceans for the first time since the LGM (Beal et al., 2011; Peeters et al., 2004; Sikes et al., 2017) but at intermediate depths. Enhanced $\Delta\delta^{13}C$ above 2,000 m during the ACR (Figure 3b) suggests that the ventilation of AAIW-depth waters was reduced owing to expanded sea-ice extent and/or a more equatorward position of the SHW, both of which would have suppressed upwelling (Anderson et al., 2009; Ferry et al., 2015; Kohler et al., 2014; Pahnke & Zahn, 2005). After the ACR, reinvigorated upwelling is evidenced by intermediate water $\Delta\delta^{13}C$ steadily decreasing into the Holocene (Figure 3b).

Between the YD and Holocene, our vertical profiles indicate the return of NADW to the Pacific (Figure 4a). The time-slice averaged $\Delta\delta^{18}O$ shows an increase between 2,500 and 3,300 m of ~0.5‰ (Figure 4a), with the largest changes occurring deeper (between 2,800 and 3,300 m). This indicates the presence of a water mass with properties distinguishable from SAMW and/or waters that occupied these depths up until this point. This shift was concomitant with the largest reduction in $\Delta\delta^{13}C$ of ~1.0‰ between SAMW and any depth during the deglaciation. The $\Delta\delta^{13}C$ between SAMW and 2,500 m approached zero owing to a rapid increase in $\delta^{13}C$ at 2,500 m (Figures 3b and S2). These changes coincided with the deepening of northern-sourced waters and the reformation of cold, salty NADW at the end of the deglaciation (Marson et al., 2014; Roberts et al., 2016; Sikes et al., 2017). With NADW sinking to its modern depth below the Drake Passage sill, it could reenter the Southern Ocean below a more buoyant, CO_2-rich PDW that had remained largely isolated from the atmosphere throughout the deglaciation (Curry & Oppo, 2005; Sikes et al., 2017). Further reductions in sea ice would have also deepened the isopycnal boundary separating the branches of Southern Ocean overturning to near its modern depth (Ferrari et al., 2014; Ferry et al., 2015). This combination provides a mechanism for enhanced $\Delta\delta^{18}O$ between 2,500 and 3,300 m (Figure 4a) and the rapid reduction in $\Delta\delta^{13}C$ between SAMW and 2,500 m, which suggest that CO_2 was finally released to the atmosphere from these depths as NADW reentered the Southern Ocean (Figure 6). Notably, this release of CO_2 from the mid-depths lags the second rise in atmospheric CO_2 during the YD by ~1.5 ka (Marcott et al., 2014, Figure 6), suggesting that the deep Pacific may have contributed to but was not the sole source of CO_2 to the atmosphere during the second half of the deglaciation.

5. Summary and Conclusions

Our analysis of the differences in $\delta^{18}O$ and $\delta^{13}C$ between intermediate, deep, and abyssal depths of the interior southwest Pacific Ocean over the last 23 kyr indicates significant changes in CO_2 storage and the source of waters in the glacial Pacific Ocean. We ascribe these to circulation changes stemming from the lack of deep water input from the Atlantic Ocean as NADW shoaled above the Drake Passage sill depth (Sikes et al., 2017). The reduced range in $\Delta\delta^{18}O$ during the LGM is attributable to the incorporation of PDW into both the upper and lower branches of overturning circulation in the southwest Pacific Ocean (Figure 2). Enhanced $\Delta\delta^{13}C$ below 1,100 m in our transect and ~940 m regionally suggests that not only was there greater storage of CO_2 in the deep ocean but that the depth of that CO_2 storage also shoaled during the

LGM (Figures 3b, 3d, and 5). Moreover, strong $\Delta\delta^{13}C$ contrasts in waters between 940 and 1,400 m and waters at and below 1,600 m highlight the presence of an isolated GAAIW distinct from the CO_2-rich CDW cell below it, both of which sat below a fresher glacial SAMW (Figure 2).

HS1 brought dramatic changes in $\Delta\delta^{18}O$ at 1,600 m while there was little change at 1,100 m (Figure 3a). We suggest this reflects the injection of cold, fresh sea-ice meltwater to the region of AAIW formation brought on by the reduction of sea ice and the northward transport of sea-ice meltwater as the westerlies shifted poleward (Anderson et al., 2009; Ferry et al., 2015; Sikes et al., 2009, Figure S5). This would have released CO_2 from the upper 1,600 m, which was likely the dominant source of respired CO_2 comprising the two pulses of rapid atmospheric CO_2 rise during HS1 (Figure 6). Gradual deep water ventilation contributed to the steady increase in atmospheric CO_2 beginning at the end of the LGM (Marcott et al., 2014; Monnin et al., 2001; Parrenin et al., 2013, Figure 6). During the Holocene, increased $\Delta\delta^{18}O$ between 2,500 and 3,300 m to modern values marks the reintroduction of NADW in the Southern Ocean (Figures 3a and 4a). This coincided with a rapid reduction in $\Delta\delta^{13}C$, the largest of the deglaciation, suggesting the remainder of the CO_2 release was associated with this profound circulation change (Sikes et al., 2017).

Our vertical oxygen isotope difference calculations indicate a two-phase change in southwest Pacific Ocean structure during the deglaciation for which circulation, buoyancy, and subsurface water mass formation were influenced first by regional sea-ice dynamics and later by changes in the delivery of North Atlantic-sourced water to the Pacific as the depth of NADW varied with climate. Overall, our isotope difference calculations identify a close coupling between changes in the vertical structure of the southwest Pacific Ocean and the loss of CO_2 to the atmosphere following the LGM.

Acknowledgments
This work was funded in part by NSF grants OCE-1159080, OCE-0823487, and OCE-0425053 to E. L. S. Thanks to David Lund and participants at the OC3 meeting in Cambridge for fruitful discussions that improved this manuscript. We thank Eli Hunter for assistance with MATLAB. We would thank the Editor, Ellen Thomas, who shepherded this manuscript through a lengthy review processes, and an anonymous reviewer for feedback that greatly strengthened this paper. All data used in this paper are archived under the original publication with the NOAA Centers for Environmental Information in the online paleoclimate database: http://www.ncdc.noaa.gov/data-access/paleoclimatology-data.

References

Abernathey, R., Marshall, J., & Ferreira, D. (2011). The dependence of Southern Ocean meridional overturning on wind stress. *Journal of Physical Oceanography*, *41*(12), 2261–2278. https://doi.org/10.1175/JPO-D-11-023.1

Abernathey, R. P., Cerovecki, I., Holland, P. R., Newsom, E., Mazlo, M., & Talley, L. D. (2016). Water-mass transformation by sea ice in the upper branch of the Southern Ocean overturning. *Nature Geoscience*, *9*(8), 596–601. https://doi.org/10.1038/ngeo2749

Adkins, J. F. (2013). The role of deep ocean circulation in setting glacial climates. *Paleoceanography*, *28*, 539–561. https://doi.org/10.1002/palo.20046

Adkins, J. F., Mcintyre, K., & Schrag, D. P. (2002). The salinity, temperature, and $\delta^{18}O$ of the glacial deep ocean. *Science*, *298*(5599), 1769–1773. https://doi.org/10.1126/science.1076252

Allen, K. A., Sikes, E. L., Hönisch, B., Elmore, A. C., Guilderson, T. P., Rosenthal, Y., & Anderson, R. F. (2015). Southwest Pacific deep water carbonate chemistry linked to high southern latitude climate and atmospheric CO_2 during the last glacial termination. *Quaternary Science Reviews*, *122*, 180–191. https://doi.org/10.1016/j.quascirev.2015.05.007

Anderson, R. F., Ali, S., Bradtmiller, L. I., Nielsen, S. H. H., Fleisher, M. Q., Anderson, B. E., & Burckle, L. H. (2009). Wind-driven upwelling in the Southern Ocean and the deglacial rise in atmospheric CO_2. *Science*, *323*(5920), 1443–1448. https://doi.org/10.1126/science.1167441

Basak, C., Frollje, H., Lamy, F., Gersonde, R., Benz, V., Anderson, R. F., et al. (2018). Breakup of last glacial deep stratification in the South Pacific. *Science*, *359*(6378), 900–904. https://doi.org/10.1126/science.aao2473

Bauska, T. K., Baggenstos, D., Brook, E. J., Mix, A. C., Marcott, S. A., Petrenko, V. V., et al. (2016). Carbon isotopes characterize rapid changes in atmospheric carbon dioxide during the last deglaciation. *Proceedings of the National Academy of Sciences*, *113*(13), 3465–3470. https://doi.org/10.1073/pnas.1513868113

Beal, L. M., De Ruijter, W. P. M., Biastoch, A., Zahn, R., & Grp, S. W. I. W. (2011). On the role of the Agulhas system in ocean circulation and climate. *Nature*, *472*(7344), 429–436. https://doi.org/10.1038/nature09983

Belkin, I. M., & Gordon, A. L. (1996). Southern Ocean fronts from the Greenwich meridian to Tasmania. *Journal of Geophysical Research*, *101*(C2), 3675–3696. https://doi.org/10.1029/95JC02750

Benz, V., Esper, O., Gersonde, R., Lamy, F., & Tiedemann, R. (2016). Last Glacial Maximum sea surface temperature and sea-ice extent in the Pacific sector of the Southern Ocean. *Quaternary Science Reviews*, *146*, 216–237. https://doi.org/10.1016/j.quascirev.2016.06.006

Bostock, H. C., Opdyke, B. N., Gagan, M. K., & Fifield, L. K. (2004). Carbon isotope evidence for changes in Antarctic intermediate water circulation and ocean ventilation in the southwest Pacific during the last deglaciation. *Paleoceanography*, *19*, PA4013. https://doi.org/10.1029/2004PA001047

Bova, S. C., Herbert, T., Rosenthal, Y., Kalansky, J., Altabet, M. A., Chazen, C., et al. (2015). Links between eastern equatorial Pacific stratification and atmospheric CO_2 rise during the last deglaciation. *Paleoceanography*, 1407–1424. https://doi.org/10.1002/2015PA002816

Boyle, E. A. (1988). Vertical oceanic nutrient fractionation and glacial/interglacial CO_2 cycles. *Nature*, *331*(6151), 55–56. https://doi.org/10.1038/331055a0

Broecker, W. S. (1982). Ocean geochemistry during glacial time. *Geochimica et Cosmochimica Acta*, *46*(10), 1689–1705. https://doi.org/10.1016/0016-7037(82)90110-7

Broecker, W. S., & Maier-Reimer, E. (1992). The influence of air-sea exchange on the carbon isotope distribution in the sea. *Global Biogeochemical Cycles*, *6*(3), 315–320. https://doi.org/10.1029/92GB01672

Burke, A., Stewart, A. L., Adkins, J. F., Ferrari, R., Jansen, M. F., & Thompson, A. F. (2015). The glacial mid-depth radiocarbon bulge and its implications for the overturning circulation. *Paleoceanography*, *30*, 1021–1039. https://doi.org/10.1002/2015PA002778

Charles, C. D., & Fairbanks, R. G. (1992). Evidence from Southern Ocean sediments for the effect of North Atlantic deep-water flux on climate. *Nature*, *355*(6359), 416–419. https://doi.org/10.1038/355416a0

Charles, C. D., Wright, J. D., & Fairbanks, R. G. (1993). Thermodynamic influences on the marine carbon isotope record. *Paleoceanography*, *8*(6), 691–697. https://doi.org/10.1029/93PA01803

Craig, H., & Gordon, L. I. (1965). Deuterium and oxygen 18 variations in the ocean and the marine atmosphere. In E. Tongiorgi (Ed.), *Stable isotopes in paleoceanographic studies and paleotemperatures*, (pp. 9–130). Italy: Cons. Naz. di Rech, Spoeto.

Curry, W. B., Duplessy, J. C., Labeyrie, L. D., & Shackleton, N. J. (1988). Changes in the distribution of $\delta^{13}C$ of deep water ΣCO_2 between the last glaciation and the Holocene. *Paleoceanography*, *3*(3), 317–341. https://doi.org/10.1029/PA003i003p00317

Curry, W. B., & Oppo, D. W. (2005). Glacial water mass geometry and the distribution of $\delta^{13}C$ of ΣCO_2 in the western Atlantic Ocean. *Paleoceanography*, *20*, PA1017. https://doi.org/10.1029/2004PA001021

De Lavergne, C., Madec, G., Roquet, F., Holmes, R. M., & McDougall, T. J. (2017). Abyssal ocean overturning shaped by seafloor distribution. *Nature*, *551*(7679), 181–186. https://doi.org/10.1038/nature24472

Denton, G. H., Anderson, R. F., Toggweiler, J. R., Edwards, R. L., Schaefer, J. M., & Putnam, A. E. (2010). The last glacial termination. *Science*, *328*(5986), 1652–1656. https://doi.org/10.1126/science.1184119

Du, J. H., Haley, B. A., Mix, A. C., Walczak, M. H., & Praetorius, S. K. (2018). Flushing of the deep Pacific Ocean and the deglacial rise of atmospheric CO_2 concentrations. *Nature Geoscience*, *11*(10), 749–755. https://doi.org/10.1038/s41561-018-0205-6

Duffy, P. B., Eby, M., & Weaver, A. J. (2001). Climate model simulations of effects of increased atmospheric CO_2 and loss of sea ice on ocean salinity and tracer uptake. *Journal of Climate*, *14*(4), 520–532. https://doi.org/10.1175/1520-0442(2001)014<0520:CMSOEO>2.0.CO;2

Duplessy, J.-C., Shackleton, N. J., Fairbanks, R. G., Labeyrie, L. D., Oppo, D., & Kallel, N. (1988). Deepwater source variations during the last climatic cycle and their impact on the global deepwater circulation. *Paleoceanography*, *3*(3), 343–360. https://doi.org/10.1029/PA003i003p00343

Elderfield, H., Ferretti, P., Greaves, M., Crowhurst, S. J., McCave, I. N., Hodell, D. a., & Piotrowski, A. M. (2012). Evolution of ocean temperature. *Science*, *337*(6095), 704–709. https://doi.org/10.1126/science.1221294

Elderfield, H., Greaves, M., Barker, S., Hall, I. R., Tripati, A., Ferretti, P., et al. (2010). A record of bottom water temperature and seawater $\delta^{18}O$ for the Southern Ocean over the past 440 kyr based on Mg/Ca of benthic foraminiferal *Uvigerina* spp. *Quaternary Science Reviews*, *29*(1–2), 160–169. https://doi.org/10.1016/j.quascirev.2009.07.013

Elmore, A. C., McClymont, E. L., Elderfield, H., Kender, S., Cook, M. R., Leng, M. J., et al. (2015). Antarctic intermediate water properties since 400 ka recorded in infaunal (*Uvigerina peregrina*) and epifaunal (*Planulina wuellerstorfi*) benthic foraminifera. *Earth and Planetary Science Letters*, *428*, 193–203. https://doi.org/10.1016/j.epsl.2015.07.013

Fairbanks, R. G. (1989). A 17,000-yearglacio-eustatic sea level record: Influence of glacial melting rates on the Younger Dryas event and deep-ocean circulation. *Nature*, *342*(6250), 637–642. https://doi.org/10.1038/342637a0

Fairbanks, R. G., Charles, C. D., & Wright, J. D. (1992). Origin of global meltwater pulses. In R. E. Taylor, et al. (Eds.), *Radiocarbon after four decades*, (pp. 473–500). Berlin: Springer-Verlag.

Ferrari, R., Jansen, M. F., Adkins, J. F., Burke, A., Stewart, A. L., & Thompson, A. F. (2014). Antarctic sea ice control on ocean circulation in present and glacial climates. *Proceedings of the National Academy of Sciences*, *111*(24), 8753–8758. https://doi.org/10.1073/pnas.1323922111

Ferry, A. J., Crosta, X., Quilty, P. G., Fink, D., Howard, W., & Armand, L. K. (2015). First records of winter sea ice concentration in the southwest Pacific sector of the Southern Ocean. *Paleoceanography*, *30*, 1525–1539. https://doi.org/10.1002/2014PA002764

Garabato, A. C. N., Polzin, K. L., King, B. A., Heywood, K. J., & Visbeck, M. (2004). Widespread intense turbulent mixing in the Southern Ocean. *Science*, *303*(5655), 210–213.

Garcia, J. L., Kaplan, M. R., Hall, B. L., Schaefer, J. M., Vega, R. M., Schwartz, R., & Finkel, R. (2012). Glacier expansion in southern Patagonia throughout the Antarctic cold reversal. *Geology*, *40*(9), 859–862. https://doi.org/10.1130/G33164.1

Gherardi, J. M., Labeyrie, L., Nave, S., Francois, R., McManus, J. F., & Cortijo, E. (2009). Glacial-interglacial circulation changes inferred from $^{231}Pa/^{230}Th$ sedimentary record in the North Atlantic region. *Paleoceanography*, *24*, PA2204. https://doi.org/10.1029/2008PA001696

Gordon, A. L. (1971). Oceanography of Antarctic waters. In J. L. Ried (Ed.), *Antarctic oceanology I*, *AGU Antarctic Research Series*, (Vol. 15), 169–203. Washington, DC: American Geophysical Union.

Gordon, A. L. (2001). Bottom water formation. In J. Steel, S. Thorpe, & K. Turekian (Eds.), *Encyclopedia of ocean sciences*, (pp. 334–340). Elsevier: Amsterdam. https://doi.org/10.1006/rwos.2001.0006

Groeskamp, S., Abernathey, R. P., & Klocker, A. (2016). Water mass transformation by cabbeling and thermobaricity. *Geophysical Research Letters*, *43*, 10,835–10,845. https://doi.org/10.1002/2016GL070860

Hain, M. P., Sigman, D. M., & Haug, G. H. (2014). Distinct roles of the Southern Ocean and North Atlantic in the deglacial atmospheric radiocarbon decline. *Earth and Planetary Science Letters*, *394*, 198–208. https://doi.org/10.1016/j.epsl.2014.03.020

Hanawa, K., & Talley, L. D. (2001). Mode waters. In G. Seidler, J. Church, & J. Gould (Eds.), *Ocean circulation and climate*, *International Geophysical Series*, (pp. 373–386). San Diego, CA: Academic Press. https://doi.org/10.1016/S0074-6142(01)80129-7

Hartin, C. A., Fine, R. A., Sloyan, B. M., Talley, L. D., Chereskin, T. K., & Happell, J. (2011). Formation rates of subantarctic mode water and Antarctic intermediate water within the South Pacific. *Deep-Sea Research Part I: Oceanographic Research Papers*, *58*(5), 524–534. https://doi.org/10.1016/j.dsr.2011.02.010

Hasson, A., Koch-Larrouy, A., Morrow, R., Juza, M., & Penduff, T. (2012). The origin and fate of mode water in the southern Pacific Ocean. *Ocean Dynamics*, *62*(3), 335–354. https://doi.org/10.1007/s10236-011-0507-3

Haumann, F. A., Gruber, N., Münnich, M., Frenger, I., & Kern, S. (2016). Sea-ice transport driving Southern Ocean salinity and its recent trends. *Nature*, *537*(7618), 89–92. https://doi.org/10.1038/nature19101

Hertzberg, J. E., Lund, D. C., Schmittner, A., & Skrivanek, A. L. (2016). Evidence for a biological pump driver of atmospheric CO_2 rise during Heinrich Stadial 1. *Geophysical Research Letters*, *43*, 12,242–212,251. https://doi.org/10.1002/2016GL070723

Ito, T., & Marshall, J. (2008). Control of lower-limb overturning circulation in the Southern Ocean by diapycnal mixing and mesoscale eddy transfer. *Journal of Physical Oceanography*, *38*(12), 2832–2845. https://doi.org/10.1175/2008JPO3878.1

Jansen, M. F. (2017). Glacial ocean circulation and stratification explained by reduced atmospheric temperature. *Proceedings of the National Academy of Sciences of the United States of America*, *114*(1), 45–50. https://doi.org/10.1073/pnas.1610438113

Keeling, R. F., & Stephens, B. B. (2001). Antarctic sea ice and the control of Pleistocene climate instability. *Paleoceanography*, *16*(1), 112–131. https://doi.org/10.1029/2000PA000529

Kobayashi, H., Abe-Ouchi, A., & Oka, A. (2015). Role of Southern Ocean stratification in glacial atmospheric CO_2 reduction evaluated by a three-dimensional ocean general circulation model. *Paleoceanography*, *30*, 1202–1216. https://doi.org/10.1002/2015PA002786

Kohler, P., Knorr, G., & Bard, E. (2014). Permafrost thawing as a possible source of abrupt carbon release at the onset of the Bolling/Allerod. *Nature Communications*, *5*, 10.

Komuro, Y., & Hasumi, H. (2003). Effects of surface freshwater flux induced by sea ice transport on the global thermohaline circulation. *Journal of Geophysical Research*, *108*(C2), 3047. https://doi.org/10.1029/2002JC001476

LeGrande, A. N., & Schmidt, G. A. (2006). Global gridded data set of the oxygen isotopic composition in seawater. *Geophysical Research Letters*, *33*, L12604. https://doi.org/10.1029/2006GL026011

Lund, D. C., Adkins, J. F., & Ferrari, R. (2011). Abyssal Atlantic circulation during the Last Glacial Maximum: Constraining the ratio between transport and vertical mixing. *Paleoceanography*, *26*, PA1213. https://doi.org/10.1029/2010PA001938

Lund, D. C., Tessin, A. C., Hoffman, J. L., & Schmittner, A. (2015). Southwest Atlantic water mass evolution during the last deglaciation. *Paleoceanography*, *30*, 477–494. https://doi.org/10.1002/2014PA002657

Lynch-Stieglitz, J., Fairbanks, R. G., & Charles, C. D. (1994). Glacial-interglacial history of Antarctic intermediate water: Relative strengths of Antarctic versus Indian Ocean sources. *Paleoceanography*, *9*(1), 7–29. https://doi.org/10.1029/93PA02446

Lynch-Stieglitz, J., Stocker, T. F., Broecker, W. S., & Fairbanks, R. G. (1995). The influence of air-sea exchange on the isotopic composition of oceanic carbon: Observations and modeling. *Global Biogeochemical Cycles*, *9*(4), 653–665. https://doi.org/10.1029/95GB02574

Mackensen, A., Hubberten, H. W., Bickert, T., Fischer, G., & Fütterer, D. K. (1993). The $\delta^{13}C$ in benthic foraminiferal tests of *Fontbotia wuellerstorfi* (Schwager) relative to the $\delta^{13}C$ of dissolved inorganic carbon in Southern Ocean deep water: Implications for glacial ocean circulation models. *Paleoceanography*, *8*(5), 587–610. https://doi.org/10.1029/93PA01291

Marcott, S. A., Bauska, T. K., Buizert, C., Steig, E. J., Rosen, J. L., Cuffey, K. M., et al. (2014). Centennial-scale changes in the global carbon cycle during the last deglaciation. *Nature*, *514*(7524), 616–619. https://doi.org/10.1038/nature13799

Marshall, J., & Speer, K. (2012). Closure of the meridional overturning circulation through Southern Ocean upwelling. *Nature Geoscience*, *5*(3), 171–180. https://doi.org/10.1038/ngeo1391

Marson, J. M., Wainer, I., Mata, M. M., & Liu, Z. (2014). The impacts of deglacial meltwater forcing on the South Atlantic Ocean deep circulation since the Last Glacial Maximum. *Climate of the Past*, *10*(5), 1723–1734. https://doi.org/10.5194/cp-10-1723-2014

Martin, J. H. (1990). Glacial-interglacial CO_2 change: The iron hypothesis. *Paleoceanography*, *5*(1), 1–13. https://doi.org/10.1029/PA005i001p00001

McCartney, M. S. (1977). Subantarctic mode water. In M. V. Angel (Ed.), *A voyage of discovery deep-sea research (suppl.)*, (pp. 103–119). Oxford, U.K: Pergammon.

McCave, I. N., Carter, L., & Hall, I. R. (2008). Glacial-interglacial changes in water mass structure and flow in the SW Pacific Ocean. *Quaternary Science Reviews*, *27*(19-20), 1886–1908. https://doi.org/10.1016/j.quascirev.2008.07.010

Menviel, L., Spence, P., Yu, J., Chamberlain, M. A., Matear, R. J., Meissner, K. J., & England, M. H. (2018). Southern Hemisphere westerlies as a driver of the early deglacial atmospheric CO_2 rise. *Nature Communications*, *9*, 12.

Monnin, E., Indermuhle, A., Dallenbach, A., Fluckiger, J., Stauffer, B., Stocker, T. F., et al. (2001). Atmospheric CO_2 concentrations over the last glacial termination. *Science*, *291*(5501), 112–114. https://doi.org/10.1126/science.291.5501.112

Ninnemann, U. S., & Charles, C. D. (2002). Changes in the mode of Southern Ocean circulation over the last glacial cycle revealed by foraminiferal stable isotopic variability. *Earth and Planetary Science Letters*, *201*(2), 383–396. https://doi.org/10.1016/S0012-821X(02)00708-2

Orsi, H., Whitworth, T., & Jr, W. D. N. (1995). On the meridional extent and fronts of the Antarctic Circumpolar Current pronounced meridional gradients in surface properties separate waters of the Southern Ocean from the warmer and saltier waters of the subtropical circulations. *Deep-Sea Research*, *42*(5), 641–673. https://doi.org/10.1016/0967-0637(95)00021-W

Pahnke, K., & Zahn, R. (2005). Southern Hemisphere water mass conversion linked with North Atlantic climate variability. *Science*, *307*(5716), 1741–1746. https://doi.org/10.1126/science.1102163

Parrenin, F., Masson-Delmotte, V., Kohler, P., Raynaud, D., Paillard, D., Schwander, J., et al. (2013). Synchronous change of atmospheric CO_2 and Antarctic temperature during the last deglacial warming. *Science*, *339*(6123), 1060–1063. https://doi.org/10.1126/science.1226368

Peeters, F. J. C., Acheson, R., Brummer, G. J. A., De Ruijter, W. P. M., Schneider, R. R., Ganssen, G. M., et al. (2004). Vigorous exchange between the Indian and Atlantic oceans at the end of the past five glacial periods. *Nature*, *430*(7000), 661–665. https://doi.org/10.1038/nature02785

Peltier, W. R., & Fairbanks, R. G. (2006). Global glacial ice volume and Last Glacial Maximum duration from an extended Barbados sea level record. *Quaternary Science Reviews*, *25*(23–24), 3322–3337. https://doi.org/10.1016/j.quascirev.2006.04.010

Piola, A. R., & Georgi, D. T. (1982). Circumpolar properties of Antarctic intermediate water and sub-Antarctic mode water. *Deep-Sea Research Part A-Oceanographic Research Papers*, *29*(6), 687–711. https://doi.org/10.1016/0198-0149(82)90002-4

Putnam, A. E., Denton, G. H., Schaefer, J. M., Barrell, D. J. A., Andersen, B. G., Finkel, R. C., et al. (2010). Glacier advance in southern middle-latitudes during the Antarctic cold reversal. *Nature Geoscience*, *3*(10), 700–704. https://doi.org/10.1038/ngeo962

Reimer, P. J., Bard, E., Bayliss, A., Beck, J. W., Blackwell, P. G., Ramsey, C. B., et al. (2013). IntCal13 and MARINE13 radiocarbon age calibration curves 0-50000 years calBP. *Radiocarbon*, *55*(04), 1869–1887. https://doi.org/10.2458/azu_js_rc.2455.16947

Rintoul, S. R., & England, M. H. (2002). Ekman transport dominates local air-sea fluxes in driving variability of subantarctic mode water. *Journal of Physical Oceanography*, *32*(5), 1308–1321. https://doi.org/10.1175/1520-0485(2002)032<1308:ETDLAS>2.0.CO;2

Roberts, J., Gottschalk, J., Skinner, L. C., Peck, V. L., Kender, S., Elderfield, H., et al. (2016). Evolution of South Atlantic density and chemical stratification across the last deglaciation. *Proceedings of the National Academy of Sciences of the United States of America*, *113*(3), 514–519. https://doi.org/10.1073/pnas.1511252113

Rohling, E. J., & Bigg, G. R. (1998). Paleosalinity and $\delta^{18}O$: A critical assessment. *Journal of Geophysical Research*, *103*(C1), 1307–1318. https://doi.org/10.1029/97JC01047

Rohling, E. J., Foster, G. L., Grant, K. M., Marino, G., Roberts, A. P., Tamisiea, M. E., & Williams, F. (2014). Sea-level and deep-sea-temperature variability over the past 5.3 million years. *Nature*, *508*(7497), 477–482. https://doi.org/10.1038/nature13230

Ronge, T. A., Steph, S., Tiedemann, R., Prange, M., Merkel, U., Nürnberg, D., & Kuhn, G. (2015). Pushing the boundaries: Glacial/interglacial variability of intermediate and deep waters in the southwest Pacific over the last 350,000 years. *Paleoceanography*, *30*, 23–38. https://doi.org/10.1002/2014PA002727

Ronge, T. A., Tiedemann, R., Lamy, F., Kohler, P., Alloway, B. V., De Pol-Holz, R., et al. (2016). Radiocarbon constraints on the extent and evolution of the South Pacific glacial carbon pool. *Nature Communications*, *7*, 11.

Rose, K. A., Sikes, E. L., Guilderson, T. P., Shane, P., Hill, T. M., Zahn, R., & Spero, H. J. (2010). Upper-ocean-to-atmosphere radiocarbon offsets imply fast deglacial carbon dioxide release. *Nature*, *466*(7310), 1093–1097. https://doi.org/10.1038/nature09288

Ruan, X. Z., Thompson, A. F., Flexas, M. M., & Sprintall, J. (2017). Contribution of topographically generated submesoscale turbulence to Southern Ocean overturning. *Nature Geoscience*, *10*(11), 840–845. https://doi.org/10.1038/ngeo3053

Saenko, O. A., Schmittner, A., & Weaver, A. J. (2002). On the role of wind-driven sea ice motion on ocean ventilation. *Journal of Physical Oceanography*, *32*(12), 3376–3395. https://doi.org/10.1175/1520-0485(2002)032<3376:OTROWD>2.0.CO;2

Saenko, O. A., & Weaver, A. J. (2001). Importance of wind-driven sea ice motion for the formation of Antarctic intermediate water in a global climate model. *Geophysical Research Letters*, *28*(21), 4147–4150. https://doi.org/10.1029/2001GL013632

Sallee, J. B., Speer, K., Rintoul, S., & Wijffels, S. (2010). Southern Ocean thermocline ventilation. *Journal of Physical Oceanography*, *40*(3), 509–529. https://doi.org/10.1175/2009JPO4291.1

Sallee, J. B., Wienders, N., Speer, K., & Morrow, R. (2006). Formation of subantarctic mode water in the southeastern Indian Ocean. *Ocean Dynamics*, *56*(5–6), 525–542. https://doi.org/10.1007/s10236-005-0054-x

Santoso, A., & England, M. H. (2004). Antarctic intermediate water circulation and variability in a coupled climate model. *Journal of Physical Oceanography*, *34*(10), 2160–2179. https://doi.org/10.1175/1520-0485(2004)034<2160:AIWCAV>2.0.CO;2

Schmitt, J., Schneider, R., Elsig, J., Leuenberger, D., Lourantou, A., Chappellaz, J., et al. (2012). Carbon isotope constraints on the deglacial CO rise from ice cores. *Science*, *336*(6082), 711–714. https://doi.org/10.1126/science.1217161

Schrag, D. P., Adkins, J. F., McIntyre, K., Alexander, J. L., Hodell, D. A., Charles, C. D., & McManus, J. F. (2002). The oxygen isotopic composition of seawater during the Last Glacial Maximum. *Quaternary Science Reviews*, *21*(1-3), 331–342. https://doi.org/10.1016/S0277-3791(01)00110-X

Shane, P., Sikes, E. L., & Guilderson, T. P. (2006). Tephra beds in deep-sea cores off northern New Zealand: Implications for the history of Taupo volcanic zone, Mayor Island and White Island volcanoes. *Journal of Volcanology and Geothermal Research*, *154*(3-4), 276–290. https://doi.org/10.1016/j.jvolgeores.2006.03.021

Shemesh, A., Hodell, D., Crosta, X., Kanfoush, S., Charles, C., & Guilderson, T. (2002). Sequence of events during the last deglaciation in Southern Ocean sediments and Antarctic ice cores. *Paleoceanography*, *17*(4), 1056. https://doi.org/10.1029/2000PA000599

Siani, G., Michel, E., De Pol-Holz, R., DeVries, T., Lamy, F., Carel, M., et al. (2013). Carbon isotope records reveal precise timing of enhanced Southern Ocean upwelling during the last deglaciation. *Nature Communications*, *4*, 9.

Sigman, D. M., & Boyle, E. A. (2000). Glacial-interglacial variations in atmospheric carbon dioxide. *Nature*, *407*(6806), 859–869. https://doi.org/10.1038/35038000

Sigman, D. M., Hain, M. P., & Haug, G. H. (2010). The polar ocean and glacial cycles in atmospheric CO_2 concentration. *Nature*, *466*(7302), 47–55. https://doi.org/10.1038/nature09149

Sikes, E. L., Allen, K. A., & Lund, D. C. (2017). Enhanced $\delta^{13}C$ and $\delta^{18}O$ differences between the South Atlantic and South Pacific during the last glaciation: The deep gateway hypothesis. *Paleoceanography*, *32*, 1000–1017. https://doi.org/10.1002/2017PA003118

Sikes, E. L., Cook, M. S., & Guilderson, T. P. (2016). Reduced deep ocean ventilation in the southern Pacific Ocean during the last glaciation persisted into the deglaciation. *Earth and Planetary Science Letters*, *438*, 130–138. https://doi.org/10.1016/j.epsl.2015.12.039

Sikes, E. L., Elmore, A. C., Allen, K. A., Cook, M. S., & Guilderson, T. P. (2016). Glacial water mass structure and rapid $\delta^{18}O$ and $\delta^{13}C$ changes during the last glacial termination in the southwest Pacific. *Earth and Planetary Science Letters*, *456*, 87–97. https://doi.org/10.1016/j.epsl.2016.09.043

Sikes, E. L., & Guilderson, T. P. (2016). Southwest Pacific Ocean surface reservoir ages since the last glaciation: Circulation insights from multiple-core studies. *Paleoceanography*, *31*, 298–310. https://doi.org/10.1002/2015PA002855

Sikes, E. L., Howard, W. R., Samson, C. R., Mahan, T. S., Robertson, L. G., & Volkman, J. K. (2009). Southern Ocean seasonal temperature and subtropical front movement on the south Tasman rise in the late quaternary. *Paleoceanography*, *24*, PA2201. https://doi.org/10.1029/2008PA001659

Sikes, E. L., Samson, C. R., Guilderson, T. P., & Howard, W. R. (2000). Old radiocarbon ages in the southwest Pacific Ocean during the last glacial period and deglaciation. *Nature*, *405*(6786), 555–559. https://doi.org/10.1038/35014581

Skinner, L., McCave, I. N., Carter, L., Fallon, S., Scrivner, A. E., & Primeau, F. (2015). Reduced ventilation and enhanced magnitude of the deep Pacific carbon pool during the last glacial period. *Earth and Planetary Science Letters*, *411*, 45–52. https://doi.org/10.1016/j.epsl.2014.11.024

Skinner, L. C., Primeau, F., Freeman, E., de la Fuente, M., Goodwin, P. A., Gottschalk, J., et al. (2017). Radiocarbon constraints on the glacial ocean circulation and its impact on atmospheric CO_2. *Nature Communications*, *8*, 10.

Skinner, L. C., Scrivner, A. E., Vance, D., Barker, S., Fallon, S., & Waelbroeck, C. (2013). North Atlantic versus Southern Ocean contributions to a deglacial surge in deep ocean ventilation. *Geology*, *41*(6), 667–670. https://doi.org/10.1130/G34133.1

Skinner, L. C., & Shackleton, N. J. (2005). An Atlantic lead over Pacific deep-water change across termination I: Implications for the application of the marine isotope stage stratigraphy. *Quaternary Science Reviews*, *24*(5–6), 571–580. https://doi.org/10.1016/j.quascirev.2004.11.008

Sloyan, B. M., & Rintoul, S. R. (2001). Circulation, renewal, and modification of Antarctic mode and intermediate water. *Journal of Physical Oceanography*, *31*(4), 1005–1030. https://doi.org/10.1175/1520-0485(2001)031<1005:CRAMOA>2.0.CO;2

Sloyan, B. M., Talley, L. D., Chereskin, T. K., Fine, R., & Holte, J. (2010). Antarctic intermediate water and subantarctic mode water formation in the southeast Pacific: The role of turbulent mixing. *Journal of Physical Oceanography*, *40*(7), 1558–1574. https://doi.org/10.1175/2010JPO4114.1

Speich, S., Blanke, B., de Vries, P., Drijfhout, S., Doos, K., Ganachaud, A., & Marsh, R. (2002). Tasman leakage: A new route in the global ocean conveyor belt. *Geophysical Research Letters*, *29*(10), 1416. https://doi.org/10.1029/2001GL014586

Stephens, B. B., & Keeling, R. F. (2000). The influence of Antarctic sea ice on glacial-interglacial CO_2 variations. *Nature*, *404*(6774), 171–174 . https://doi.org/10.1038/35004556

Stern, J. V., & Lisiecki, L. E. (2014). Termination 1 timing in radiocarbon-dated regional benthic $\delta^{18}O$ stacks. *Paleoceanography*, *29*, 1127–1142. https://doi.org/10.1002/2014PA002700

Talley, L. (2013). Closure of the global overturning circulation through the Indian, Pacific, and Southern Oceans: Schematics and transports. *Oceanography*, *26*(1), 80–97. https://doi.org/10.5670/oceanog.2013.07

Talley, L. D. (2003). Shallow, intermediate, and deep overturning components of the global heat budget. *Journal of Physical Oceanography*, *33*(3), 530–560. https://doi.org/10.1175/1520-0485(2003)033<0530:SIADOC>2.0.CO;2

Tamsitt, V., Drake, H. F., Morrison, A. K., Talley, L. D., Dufour, C. O., Gray, A. R., et al. (2017). Spiraling pathways of global deep waters to the surface of the Southern Ocean. *Nature Communications*, *8*, 1–10.

Toggweiler, J. R. (2009). Shifting westerlies. *Science*, *323*(5920), 1434–1435. https://doi.org/10.1126/science.1169823

Toggweiler, J. R., & Lea, D. W. (2010). Temperature differences between the hemispheres and ice age climate variability. *Paleoceanography*, *25*, PA2212. https://doi.org/10.1029/2009PA001758

Toggweiler, J. R., Russell, J. L., & Carson, S. R. (2006). Midlatitude westerlies, atmospheric CO_2, and climate change during the ice ages. *Paleoceanography*, *21*, PA2005. https://doi.org/10.1029/2005PA001154

Toggweiler, J. R., & Samuels, B. (1993). New radiocarbon constraints on the upwelling of abyssal water to the ocean's surface. In M. Heimann (Ed.), *The global carbon cycle*. Berlin: Springer-Verlag.

Watson, A. J., & Naveira Garabato, A. C. (2006). The role of Southern Ocean mixing and upwelling in glacial-interglacial atmospheric CO_2 change. *Tellus Series B: Chemical and Physical Meteorology*, *58*(1), 73–87. https://doi.org/10.1111/j.1600-0889.2005.00167.x

Watson, A. J., Vallis, G. K., & Nikurashin, M. (2015). Southern Ocean buoyancy forcing of ocean ventilation and glacial atmospheric CO_2. *Nature Geoscience*, *8*(11), 861–864. https://doi.org/10.1038/ngeo2538

Weber, M. E., Clark, P. U., Kuhn, G., Timmermann, A., Sprenk, D., Gladstone, R., et al. (2014). Millennial-scale variability in Antarctic ice-sheet discharge during the last deglaciation. *Nature*, *510*(7503), 134–138. https://doi.org/10.1038/nature13397

Wolff, E. W., Fischer, H., Fundel, F., Ruth, U., Twarloh, B., Littot, G. C., et al. (2006). Southern Ocean sea-ice extent, productivity and iron flux over the past eight glacial cycles. *Nature*, *440*(7083), 491–496. https://doi.org/10.1038/nature04614